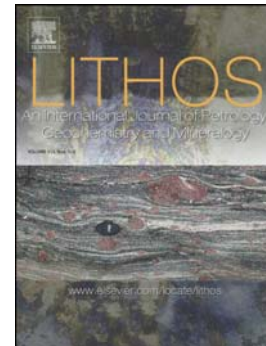


Accepted Manuscript

Geochronological, elemental and Sr-Nd-Hf-O isotopic constraints on the petrogenesis of the Triassic post-collisional granitic rocks in NW Thailand and its Paleotethyan implications

Yuejun Wang, Huiying He, Peter A Cawood, Weiming Fan, Boontarika Srithai, Qinlai Feng, Yuzhi Zhang, Xin Qian



PII: S0024-4937(16)30295-X

DOI: doi: [10.1016/j.lithos.2016.09.012](https://doi.org/10.1016/j.lithos.2016.09.012)

Reference: LITHOS 4073

To appear in: *LITHOS*

Received date: 10 June 2016

Accepted date: 8 September 2016

Please cite this article as: Wang, Yuejun, He, Huiying, Cawood, Peter A, Fan, Weiming, Srithai, Boontarika, Feng, Qinlai, Zhang, Yuzhi, Qian, Xin, Geochronological, elemental and Sr-Nd-Hf-O isotopic constraints on the petrogenesis of the Triassic post-collisional granitic rocks in NW Thailand and its Paleotethyan implications, *LITHOS* (2016), doi: [10.1016/j.lithos.2016.09.012](https://doi.org/10.1016/j.lithos.2016.09.012)

This is a PDF file of an unedited manuscript that has been accepted for publication. As a service to our customers we are providing this early version of the manuscript. The manuscript will undergo copyediting, typesetting, and review of the resulting proof before it is published in its final form. Please note that during the production process errors may be discovered which could affect the content, and all legal disclaimers that apply to the journal pertain.

Geochronological, elemental and Sr-Nd-Hf-O isotopic constraints on the petrogenesis of the Triassic post-collisional granitic rocks in NW Thailand and its Paleotethyan implications

Yuejun Wang^{1, 2,*}, Huiying He¹, Peter A Cawood³ Weiming Fan²,
Boontarika Srithai⁴ Qinlai Feng⁵ Yuzhi Zhang¹, Xin Qian¹

1 School of Earth Science and Geological Engineering, Sun Yat-sen University, Guangzhou 510275, China

2 CAS Center for Excellence in Tibetan Plateau Earth Sciences, Beijing 100101, China

3 Department of Earth Sciences, University of St Andrews, North Street, St Andrews KY169AL, UK

4 Department of Geological Sciences, Faculty of Science, Chiang Mai University, Chiang Mai 50200, Thailand

5 State Key Laboratory of Geological Processes and Mineral Resources, Faculty of Earth Sciences, China University of Geosciences, Wuhan, 430074, China

* Corresponding author

Current address: School of Earth Science and Geological Engineering

Sun Yat-sen University

No. 135, Xingang Xi Road, Guangzhou, 510275

People's Republic of China

Tel: 86-20-84111209

email: wangyuejun@mail.sysu.edu.cn

Abstract New U-Pb geochronological, petrologic, elemental and Sr-Nd-Hf-O isotopic data for the granites from the Inthanon and Sukhothai zones in NW Thailand in conjunction with correlations with SW China are presented to constrain the age and position of the Paleotethys Ocean in this region and the associated assembly of Southeast Asia. The geochronological data show that the granitic rocks in the Inthanon and Sukhothai zones, herein named Group 1 and Group 2 granites, respectively, yield similar crystallization ages of 230-200 Ma. Group 1 samples are characterized by monzogranite and granite with I- and S-type geochemical affinity and Group 2 samples by I-type monzogranite and granodiorite. They have generally similar chondrite-normalized REE and PM- normalized multi-element patterns but distinct Sr-Nd-Hf-O isotopic compositions. Group 1 samples have slightly higher initial $^{87}\text{Sr}/^{86}\text{Sr}$ ratios (0.7111- 0.7293) but lower $\varepsilon_{\text{Nd}}(t)$ values (-11.1~ -14.1) than those of Group 2 samples ($^{87}\text{Sr}/^{86}\text{Sr}_{(i)}=0.7073-0.7278$ and $\varepsilon_{\text{Nd}}(t)=-8.3\sim -11.0$). Group 1 samples show the lower $\varepsilon_{\text{Hf}}(t)$ values (-5.4 ~ -18.2), older T_{DM} (1.62-2.40 Ga) and higher $\delta^{18}\text{O}$ values (+7.95-+9.94) than those of Group 2 samples ($\varepsilon_{\text{Hf}}(t)$ of -11.1-+4.80, T_{DM} of 0.96-1.95 Ga and $\delta^{18}\text{O}$ of +4.95~+7.98) for the Triassic crystallization zircons. These geochemical signatures are similar to the Kwangolian and Indosinian granites in the South China and Indochina blocks but distinct from those of the Gangdese I-type granite and Sibumasu Paleozoic granite. Our data suggest that Group 1 samples mainly originated from the early Paleozoic supracrustal rocks containing metapelite and metavolcanic components, which had previously experienced the surface weathering. Group 2 samples were derived from a hybridized

source of an old metamorphic and a newly underplated mafic component. Synthesis of our data with available regional observations indicate that the Inthanon zone represents the main suture zone of the eastern Paleotethyan Ocean in NW Thailand and links with the Changning-Menglian suture zone in SW Yunnan (SW China). In NW Thailand, a switch from the eastward subduction of the Paleotethyan oceanic plate to the collision of the Sibumasu with Indochina blocks occurred at ~237 Ma, and syn- and post-collisional time being at ~237-230 Ma and ~200-230 Ma, respectively. The late Triassic granites in the Inthanon and Sukhothai zones are representative of the post-collisional magmatic products.

Keywords late Triassic granite, zircon U-Pb dating, elemental and Sr-Nd-Hf-O isotopic data, post-collisional collapse, eastern Paleotethyan evolution, NW Thailand

1 Introduction

The rifting, breakup and drifting of continental fragments off the northern margin of Gondwana and their accretion onto Europe and Asia from the Paleozoic to Cenozoic is recorded in the opening and closing of the Paleo- and Neotethyan and related ocean basins (e.g., Cawood et al., 2013). Remnants of the Paleotethyan Ocean extended from the European Alps through Afghanistan to southern Tibet and then southward through NW Thailand to Peninsular Malaysia and Sumatra (inset in Fig. 1; Bullard and Smith, 1965; Sengör and Hsü, 1984; Metcalfe, 1996, 2002, 2014; Metcalfe and Isozaki, 2009; Srichan et al., 2009). In Tibet and Peninsular Malaysia, the Longmucuo-Shuanghu and the Bentong–Raub suture zones (Fig. 1) highlight the

position of the eastern Paleotethyan ocean (e.g., Hutchison, 1975; Metcalfe, 1996, 2002; Zhong, 1998; Li et al., 2005; Feng et al., 2008). In the intervening region, the eastern Paleotethyan Ocean is represented by the Changning-Menglian suture in SW China that separates the Baoshan/Sibumasu and Simao/Indochina blocks (Fig. 1). It is marked by the abundant ophiolitic mélange, high-pressure metamorphic rocks and associated igneous and sedimentary rocks (e.g., Sengör, 1976; Mo et al., 1998; Zhong, 1998; Fan et al., 2015; Wang et al., 2010; Peng et al., 2006, 2014; Metcalfe, 2002; Henning et al. 2009). The southward extension of the Changning-Menglian suture zone with the Bentong–Raub zone in Peninsular Malaysia, through intervening NW Thailand (Fig. 1), is poorly constrained with the Nan suture, the Mae Yuan Fault and the Chiang Rai Fault having been proposed as potential remnants of the eastern Paleotethyan ocean in this region (Fig. 2; Barr and MacDonald, 1991; Caridroit, 1993; Bunopas, 1994; Hada et al., 1997; Ueno, 1999, 2003; Feng, 2002; Panjasawatwong et al. 2006; Ferrari et al., 2008; Hara et al., 2009; Qian et al. 2015a, 2016; Wang et al., 2016).

In NW Thailand, the granitic rocks are extensively distributed, and are believed as a segment of a giant late Paleozoic igneous belt extending through SE Asia (Figs. 1-2, Barr et al., 2000; Panjasawatwong et al., 2006). These granites, with unknown crystallization age, are potentially temporally and spatially linked to the giant igneous belt in SW Yunnan (e.g., Barr et al., 2000, 2006; Fontaine, 2002; Panjasawatwong, 2003; Zhong, 1998; Hennig et al., 2009; Wang et al., 2010; Peng et al., 2014 and references therein), thus are important carriers for probing the tectonic evolution of

the eastern Paleotethyan ocean and subsequent closure and assemblage (e.g., Pearce et al., 1984; Martin, 1987; Bonin, 2007). In this paper we constrain the position and evolution of the Paleotethyan Ocean in NW Thailand through an analysis of the granitic rocks that occur in the tectonic blocks between the Nan suture, the Chiang Rai Fault and the Mae Yuan Fault. To achieve this, we systematically studied forty-eight granitic samples from the sixteen sites in NW Thailand (e.g., Chiang Rai, Chiang Mai, Fang, Inthanon and Tak), including new U-Pb geochronological, petrologic, elemental and Sr-Nd-Hf-O isotopic data.

2 Geological setting and petrography

NW Thailand is divided from east to west into four tectonic units: the Indochina block, the Sukhothai and Inthanon zones, and the Sibumasu block, separated by the Nan suture, the Chiang Rai Fault and the Mae Yuan Fault, respectively (Figs. 2-3; Barr and Macdonald, 1991; Sone and Metcalfe, 2008).

The Indochina block lies between the Ailaoshan-Song Ma and Nan sutures (Fig. 1; Metcalfe, 1998, 2013; Lepvrier et al., 2008; Fan et al., 2010). It consists of a Proterozoic package of volcanoclastics and carbonates (Zhong, 1998) uncomfortably overlain by Paleozoic-lower Triassic carbonate and siliciclastic sequences, which display Cathaysia flora and fauna, similar to those of the Yangtze Block (Zhong, 1998; Feng, 2002; Metcalfe, 2006; Wongwanich and Boucot, 2011). Mesozoic rocks are characterized by a continental red bed sequence, such as that in the Khorat Plateau Basin (e.g., Ridd et al., 2011). The Nan suture has traditionally been interpreted as the

remnants of a Paleotethyan ocean, but more recently it has been considered to mark a back-arc basin (e.g., Ueno and Hisada, 2001; Qian et al., 2015a).

The Sibumasu block is a part of the peri-Gondwanan Cimmerian continent that lay along the northeastern margin of the supercontinent in the late Carboniferous-early Permian period (e.g., Metcalfe, 1996, 1998, 2006, 2013; Sevastjanova et al., 2011). It is also known as the Shan-Thai block in NW Thailand, the South Qiangtang block in Tibet, and the Baoshan and Tengchong blocks in SW China (e.g., Fontaine, 2002; Metcalfe, 1996, 2002, 2006, 2013). The block contains abundant granitic gneiss, migmatite and leucogranite, previously mapped as Proterozoic basement. The pre-Silurian package is uncomfortably overlain by Upper Carboniferous to Lower Permian glaciogenic diamictites and Middle-Upper Permian platform carbonates (e.g., Ueno, 2003).

The Sukhothai zone (Figs. 2-3) mainly consists of Paleozoic greywackes, shales, limestones and schists and uncomfortably-underlain middle/upper Triassic molasses and Jurassic epicontinental sedimentary rocks (Ueno and Hisada, 2001; Metcalfe, 2006, 2013; Ridd et al., 2011). In this zone, the Permian-Triassic volcanic and granitic rocks are widespread and interpreted to be generated in a continental arc setting (Barr and Macdonald, 1991; Panjasawatwong, 2003; Ridd et al., 2011; Qian et al., 2015a, 2016).

The Inthanon zone, originally proposed by Barr and Macdonald (1991), consists of metamorphic rocks of unknown age, Cambrian sandstones, Ordovician limestones, late Paleozoic carbonates, siliciclastics, cherts and basalts, and upper Triassic- Jurassic

volcanoclastics, as well as abundant Mesozoic gneissic and massive granites (Fig. 3; e.g., Feng, 2002; Feng et al., 2004, 2008; Hara et al., 2009; Ridd et al., 2011; Ridd, 2015).

Coarse- to medium-grained porphyritic and massive granites and granodiorites, as well as granitic gneisses, are widely distributed across NW Thailand (Figs. 2-3). The distribution is superimposed on the lithotectonic Indochina block, the Sukhothai and Inthanon zones, and the Sibumasu block, with Cobbing et al. (1992) subdividing the granitoids into the Western, Central and Eastern Granite Provinces separated by the Mae Yuam and Chiang Rai faults, respectively (Figs. 2-3; Hutchison, 2007; Ridd et al., 2011).

The Eastern Province extends from NW Laos through Chiang Rai, Loei and Chanihaburi in Thailand, and southerly to Peninsular Malaysia. It outcrops in the Sukhothai zone and Indochina block to the east of the Chiang Rai Fault. The granites intruded the pre-Triassic strata as stocks and batholiths, and have been previously mapped as Permo-Triassic I-type granite (Ridd et al., 2011). The Tak batholith is the representative pluton, which is mainly composed of hornblende-bearing diorite to granodiorite, monzonite, granitic porphyry and porphyritic granites.

The Western Province occurs within the Sibumasu block, to the west of the Mae Yuam Fault, and southerly extends from the border of Thailand and Myanmar into Sumatra across the Malacca Straits and Phuket Island. It has been considered to be composed of a Cretaceous and Tertiary Sn- and W-bearing S-type and I-types granites (Cobbing et al., 1992; Ridd et al., 2011).

The Central Province, located in the Inthanon zone between the Mae Yuam and Chiang Rai faults, is characterized by granitic gneiss and migmatite in the core and by granites in the flanks (e.g., Cobbing et al., 1986, 1992; Ridd et al., 2011). The granitic gneisses and migmatite, with a penetrative subhorizontal schistosity, was originally been mapped as Precambrian basement (e.g., Chakkaphak and Veeraburus, 1982). However, Dunning et al. (1995) and Cobbing el al. (1992) obtained Permian and Triassic ages (269-207 Ma) for the gneisses at Doi Inthanon (Figs. 2-3). The flanking granites are composed of medium to coarse-grained porphyritic and massive granites, K-feldspar megacrystic granites, monzonitic granites and two-mica granites, e.g., the Chiang Rai, Fang, Mae Sariang intrusions (Figs. 2-4; Mahawat, 1982; Mahawat et al. 1990).

The granitic gneiss has a mineral assemblage of K-feldspar (~35-60 vol. %), quartz (~20-35 vol. %), plagioclase (~10-25 vol. %) and biotite (~3-10 vol. %) with minor amount of accessory minerals (e.g., tourmaline, apatite, zircon, and monazite and Fe-Ti oxides), as shown in Fig. 4a-b. They contain angular to rounded paragneiss and amphibolite enclaves. The mineral composition for the massive granite includes ~10-30 vol.% plagioclase, ~20-60 vol.% K-feldspar and ~10-50 vol.% quartz (Fig. 4c-f). These granites usually show porphyritic textures with feldspar phenocrysts mostly from 3 to 8 mm, but occasionally up to 30 mm long. The matrix of the granites is mainly composed of fine-grained K-feldspar, plagioclase, quartz and minor biotite. Granodiorite and hornblende granite with mafic enclaves are observed in massive granitic batholiths in Eastern Province (e.g., Ridd et al., 2011). Locations of samples

analyzed in this paper are shown in Figure 3 and Table 1.

3 Analytical techniques

Zircon grains for U-Pb dating were separated by standard density and magnetic separation techniques at the mineral separation laboratory of the Bureau of Geology and Mineral Resources of Hebei Province. Grains were mounted in epoxy, polished and coated with gold, and then photographed in transmitted and reflected light. The internal texture of grains was examined using cathodoluminescence (CL) imaging via a scanning electron microprobe at the Sun Yat-sen University, Guangzhou.

In-situ zircon U-Th-Pb measurements and Lu-Hf isotopic analyses were undertaken using a Nu Plasma HR MC-ICPMS (Nu Instruments) with ArF-193 nm laser ablation system (Resolution M-50) at the University of Hong Kong. The zircon standards CN92-2, 91500, GJ-1 and Plešovice were used to calibrate the U-Th-Pb ratios. Silicate glass standard NIST 610 was analyzed to ensure machine optimization. The spot size for data collection was 30-40 μm . Instrument settings and a detailed outline of analytical procedures are illustrated by Xia et al. (2012) and Wu et al. (2006). Individual U-Pb analyses are presented with 1σ error. Meanwhile, uncertainties in grouped ages are quoted at the 95% confidence level. The age calculations and plots were made using the Isoplot and Squid programs of Ludwig (2003). External calibration of zircon in-situ Lu-Hf isotopes were measured using zircon standard 91500 together with analyses of unknowns, which yielded a signal intensity of ~ 10 Vat ^{180}Hf for the standard zircon 91500 with a recommended

$^{176}\text{Hf}/^{177}\text{Hf}$ ratio of 0.282293 ± 28 (Wu et al. 2006). Data were normalized to $^{176}\text{Hf}/^{177}\text{Hf}=0.7325$, using exponential correction for mass bias. The mean β_{Yb} value was applied for the isobaric interference correction of ^{176}Yb on ^{176}Hf in the same spot. The ratio of $^{176}\text{Yb}/^{172}\text{Yb}$ (0.5887) was also applied for the Yb correction. A decay constant for ^{176}Lu of $1.865 \pm 0.015 \times 10^{-11}/\text{year}$ (Scherer, 2001), the present-day chondritic ratios of $^{176}\text{Hf}/^{177}\text{Hf} = 0.282772$ and $^{176}\text{Lu}/^{177}\text{Hf} = 0.0332$ (Blichert-Toft and Albarède, 1997) were used for calculating $\epsilon\text{Hf}(t)$ values. The two-stage model age (TDM2) was also calculated on basis of $^{176}\text{Lu}/^{177}\text{Hf}=0.015$ for average continental crust (Griffin et al., 2002).

Zircon oxygen isotopic analyses were measured using the Cameca 1280 at Institute of Geology and Geophysics, Chinese Academy of Sciences (CAS). The Cs^+ ion beam was accelerated to 10 kV, with an intensity of ~ 2 nA. The normal incidence electron flood gun was used to compensate for sample charging. Oxygen isotopes were measured in multi-collector mode with two off-axis Faraday cups. Analytical procedures are similar to that described by Li et al. (2010, 2013). The internal precision of a single analysis was generally better than 0.20 ‰ (1σ) for $^{18}\text{O}/^{16}\text{O}$ ratio. Zircon U-Pb geochronological dating results and in-situ Hf-O isotopic analyzed data are listed in Supplementary Dataset and Table 2, respectively.

Whole-rock samples for elemental and Sr–Nd isotopic analyses were crushed to 200-mesh using an agate mill. The major oxides were analyzed at the Guangzhou Institute of Geochemistry (GIG), Chinese Academy of Sciences (CAS) by a Rigaku ZSX100e wavelength X-ray fluorescence spectrometry with relative standard

derivations of 5%. Trace element analyses were performed using a Perkin–Elmer Sciex ELAN 6000 ICP–MS at the GIG, CAS. The analytical precision is better 5% for elements >10 ppm, less than 8% for those <10 ppm, and about 10% for transition metals. Detailed sample preparation and analytical procedure followed Li et al. (2002). Sr and Nd isotopic analyses were carried out using a Neptune Plus multi-collection mass spectrometry equipped with nine Faraday cup collectors and eight ion counters in GIG, CAS. Details of analytical methods are presented by Yang et al. (2006). The total procedure blanks were in the range of 200–500 pg for Sr and ≤50 pg for Nd. The mass fractionation corrections for Sr and Nd isotopic ratios are based on $^{86}\text{Sr}/^{88}\text{Sr} = 0.1194$ and $^{146}\text{Nd}/^{144}\text{Nd} = 0.7219$, respectively. The measured $^{87}\text{Sr}/^{86}\text{Sr}$ ratios of the (NIST) SRM987 standard are 0.710265 ± 12 (2σ) and the measured $^{143}\text{Nd}/^{144}\text{Nd}$ ratios of the La Jolla standard are 0.511862 ± 10 (2σ). During the analytical process, within-run errors of precision are estimated to be better than 0.000015 for $^{146}\text{Nd}/^{144}\text{Nd}$ in the 95% confidence level. The whole-rock major oxides, trace elemental, as well as Sr-Nd isotopic data of the selected samples are listed in Table 3.

4 Zircon U-Pb geochronological and in-situ Hf-O isotopic results

Fourteen samples were selected for zircon U-Pb dating with ten of them also undergoing Hf-O isotopic analyses. The analytical results are summarized in Table 1. They are granitic gneisses and porphyritic and massive granites with the major minerals of feldspar, plagioclase and quartz (Fig. 4). Zircons from these samples are transparent to subtransparent prismatic grains. In CL, almost all grains show an

internal structure with oscillatory zoning and several grains contain inherited cores (Appendix 1).

4.1 Granites in the Inthanon zone (Central Province)

TG-5A and TG-6A are granitic gneisses near the Fang Hotspring National Park (Fig. 3a). Thirteen out of the 24 grains with the oscillatory zones from TG-5A yield a weighted mean age of 219 ± 2 Ma (Fig. 5a, MSWD = 0.2) with Th/U = 0.12-0.73, which give $\epsilon\text{Hf(t)}$ values of -10.9~-15.1, T_{DM} model ages of 2.2-1.9 Ga and $\delta^{18}\text{O}$ values of 8.69-9.21‰ (Tables 1-2). For TG-6A (Fig. 5b), a weighted mean age of 200 ± 2 Ma (MSWD=1.0) is defined by 9 analyses out of 22 spots with Th/U = 0.10-1.26. The remaining analytical spots for TG-5A and TG-6A plotted along or close to the concordia curve with the apparent ages of 1573-419 Ma ($n = 11$) and 2457-364 Ma ($n = 13$), respectively.

TG-30B₁, TG-52A and TG-53A are granitic gneisses from Doi Inthanon, along the Chiang Mai-Mae La Noi Road. The zircons are oscillatory zoned in CL images and have Th/U ratios of 0.10-0.86. Five spots from seven grains for TG-30B₁ give a weighted mean $^{206}\text{Pb}/^{238}\text{U}$ age of 222 ± 3 Ma (Fig. 5c; MSWD = 1.0). Thirty-five analytical spots from TG-52A and sixteen spots from TG-53A form coherent age-clusters with the weighted mean ages of 212 ± 3 Ma (MSWD = 1.4) and 207 ± 2 Ma (MSWD = 0.3), respectively (Fig. 5d-e). Their $\epsilon\text{Hf(t)}$ values, T_{DM} model ages and $\delta^{18}\text{O}$ values are in range of -21.0~-9.6, 2.57~1.86 Ga, and 8.82~9.86‰ for TG-52A, and -19.9~-10.3, 2.50~1.90 Ga, and 8.56~9.84‰ for TG-53A (Tables 1-2). The remaining fifteen analyses from these samples plot near to the concordia curve show

the older apparent ages ranging from 2544 Ma to 254 Ma, which are interpreted as inherited grains.

Porphyritic granites TL-26A and TG-11A are from Sleeping Buddha Park and Mae Wiang Pa Pao, respectively. Analytical spots TL-26A-09, TL-26A-20, TL-26A-23 and TG-11A-07 yield the U-Pb apparent ages of 1411 ± 57 Ma, 466 ± 14 Ma, 260 ± 9 Ma and 727 ± 21 Ma, respectively, which are interpreted as inherited zircons. Other analyses plot along concordia, yielding weighted mean ages of 226 ± 3 Ma ($n = 19$, MSWD = 0.6) for TL-26A, and 220 ± 1 Ma ($n = 24$, MSWD = 1.0) for TG-11A (Fig. 5f-g). Their $\epsilon\text{Hf}(t)$ values, T_{DM} model ages and $\delta^{18}\text{O}$ values for TL-26A range from -12.1 to -5.4, 2.02 Ga to 1.60 Ga, and 7.95 ‰ to 9.71 ‰.

Porphyritic granite TG-42A was collected from the 85 km Marker along Highway 1095. Spot analyses TG-42A-02 and TG-42A-17 yield apparent ages of 2432 ± 43 Ma and 890 ± 21 Ma, with negative $\epsilon\text{Hf}(t)$ values of -17.4 and -4.7, and high $\delta^{18}\text{O}$ values of 8.98 and 8.22, respectively. The remaining seventeen analyses from the sample show Th/U ratios of 0.10-0.58 and define the $^{206}\text{Pb}/^{238}\text{U}$ apparent ages of 214-206 Ma, with a weighted mean age of 210 ± 1 Ma (MSWD = 0.6; Fig. 5h). The $\epsilon\text{Hf}(t)$ values range from -17.7 to -10.3, T_{DM} model age from 2.36 Ga to 1.90 Ga, and $\delta^{18}\text{O}$ values from 8.28‰ to 9.59‰.

Granitic gneissic enclave TG-16A₂ and hosted porphyritic granite TG-16B₁ are taken from the Khun Tan pluton. The analyses for TG-16A₂ and TG-16B₁ give weighted mean $^{206}\text{Pb}/^{238}\text{U}$ ages of 237 ± 2 Ma ($n = 15$, MSWD = 0.2) and 223 ± 2 Ma ($n = 13$, MSWD = 0.7), interpreted as the crystallization ages of the enclave and

hosted granite, respectively (Fig. 5i-j). Grains from both samples have similar $\epsilon\text{Hf(t)}$ values (-15.6~ -10.9 and -16.7 ~ -11.5), T_{DM} values (2.24~1.95 Ga and 2.31~1.99 Ga), and $\delta^{18}\text{O}$ values (8.73~9.94‰ and 6.59~9.56‰). Four grains from TG-16A₂ yield older U-Pb apparent ages of 1129-507 Ma whereas five grains from TG-16B₁ have the U-Pb apparent ages of 1191-787 Ma.

4.2 Monzonitic granite in the Suhkothai zone (Eastern Province)

Analytical grains from porphyritic granite TG-8A show strong oscillatory zoning and variable Th/U ratios (0.23-2.15), indicative of an igneous origin. Nineteen U-Pb zircon analyses plot along concordia and yield a weighted mean age of 226 ± 3 Ma (Fig. 5k; MSWD = 0.9) and negative $\epsilon\text{Hf(t)}$ values of -14.4 to -6.2, corresponding with T_{DM} ages of 2.11 Ga to 1.65 Ga. $\delta^{18}\text{O}$ values range from 6.89 ‰ to 8.17 ‰ with the mean values of 7.66 ± 0.19 ‰.

Massive monzonitic granite TL-13A₁ was collected from the site of Wat Kio Kan. Twenty-five analyses of 25 grains with oscillatory zoning form two clusters. The older cluster defined by twelve spots gives a weighted mean $^{206}\text{Pb}/^{238}\text{U}$ age of 236 ± 5 Ma (MSWD = 1.0), interpreted to reflect inherited grains (Fig. 5l). Their $\epsilon\text{Hf(t)}$ values vary from +0.7 to +4.6, T_{DM} model ages from 1.23 Ga to 0.96 Ga, and $\delta^{18}\text{O}$ values from 6.02‰ to 7.16‰. Other cluster yields a weighted mean age of 216 ± 2 Ma (n=13, MSWD=1.7) with $\epsilon\text{Hf(t)}$ values of +1.2~ +4.1, T_{DM} of 1.18~1.00 Ga, and $\delta^{18}\text{O}$ values of 5.88~7.17 ‰, representing the crystallization age of the pluton.

Zircon grains from massive monzonitic granites TG-26C and TG-27A in the Tak pluton (Fig. 3) have Th/U ratios of 0.13-0.86 and 0.39-1.18, respectively. A weighted

mean age of 214 ± 1 Ma (MSWD = 0.8) is given by twenty-four analytical spots from TG-26C (Fig. 5m). Twenty-one grains of TG-27A show the $^{206}\text{Pb}/^{238}\text{U}$ apparent ages ranging from 234 Ma to 216 Ma, yielding a weighted mean age of 224 ± 2 Ma (MSWD = 0.7; Fig. 5n). The late Triassic crystallization grains exhibit the relatively high $\epsilon\text{Hf(t)}$ value of -3.2~+3.4, young T_{DM} model age of 1.04~1.47 Ga and low $\delta^{18}\text{O}$ values of 4.95~6.38‰.

5 Geochemical results

The elemental and Sr-Nd isotopic analytical results for the representative granitic samples in NW Thailand are presented in Table 3. On the basis of the sampling locations from the Inthanon (Central Province) and Sukhothai (Eastern Province) zones, these granitic samples can be spatially divided into two groups, with Group 1 constituted by 33 granitic gneisses and massive granites and Group 2 by 15 porphyritic and massive granites, respectively.

The Group 1 and 2 samples have similar major oxides compositions with $\text{SiO}_2 = 65.5\text{-}76.3$ wt%, $\text{Al}_2\text{O}_3 = 11.6\text{-}15.5$ wt%, $\text{FeOt} = 0.01\text{-}4.93$ wt%, $\text{MgO} = 0.1\text{-}2.9$ wt%, $\text{K}_2\text{O} + \text{Na}_2\text{O} = 4.9\text{-}11.4$ wt% with generally $\text{K}_2\text{O} > \text{Na}_2\text{O}$ (Table 4). Group 1 samples exhibit lower CaO but higher P_2O_5 than those of Group 2 samples at comparable SiO_2 . In the QAP diagram (Fig. 6), Group 1 samples plot in the monzogranite and granite fields whereas Group 2 samples are monzogranite with the exception of several samples plotting in the granodiorite field. Group 1 samples show high-K calc-alkaline and shoshonitic affinities but Group 2 samples correspond with the high-K

calc-alkaline series (Fig. 7a). A/CNK (molar $\text{Al}_2\text{O}_3/\text{CaO}+\text{Na}_2\text{O}+\text{K}_2\text{O}$) ratios range from 0.95 to 1.43 and A/NK (molar $\text{Al}_2\text{O}_3/\text{Na}_2\text{O}+\text{K}_2\text{O}$) ratios from 1.1 to 2.3 for Group 1 samples (Fig. 7b). Group 1 samples have CIPW-normative minerals of 22-39 vol. % Qz, 14-60 vol. % Or, 9-33 vol. % Ab, 2-11 vol. % An and 0-6 vol. % corundum. A/CNK = 0.91-1.08 and A/NK = 1.1-1.9 for Group 2 samples with Qz = 19-47 vol. %, Or = 19-33 vol. %, Ab = 12-32 vol. %, An = 4-16 vol. % and <1.5 vol. % corundum (Fig. 7b), similar to those of typical I-type granites (Chappell and White, 1974, 1992, 2001). In the plots of Ga/Al vs Zr+Nb+Ce+Y and FeOt/MgO (Figs. 7c-d), Group 1 and 2 samples fall into I-, S- and M-type rather than A-type granite field. However, the different evolved trends are given for each group with SiO_2 contents of <~72 wt% and >~72 wt%, suggestive of the distinct magma fractionation process. Zirconium, Sr, Nb, Ba and Eu decreases with increasing SiO_2 for each group.

(La/Yb)n ratios for Group 1 and 2 samples range from 6.13 to 22.5 and (Gd/Yb)n from 1.05 to 2.94 (Table 4) with the Eu/Eu* ratios of 0.30-0.61. On the primitive mantle-normalized spidergram (Fig. 8b), both groups display similar patterns with negative Sr, P, Ti, Ba and Nb anomalies and positive Pb anomalies. As shown in Table 3 and Figure 9, Group 1 samples show initial $^{87}\text{Sr}/^{86}\text{Sr}$ ratios of 0.7111-0.7293 and $\varepsilon_{\text{Nd}}(\text{t})$ values of -11.1~ -14.1, similar with those of the Indosinian and Kwangshian granites in the South China Block (SCB) and Lincang Triassic granites in SW Yunnan, but distinct from those of the Gangdese I-type granite and Sibumasu Paleozoic granite (e.g., Li and McCulloch, 1996; Shen et al., 2009; Peng et al., 2013; Wang et al., 2007, 2013, 2014 and reference therein). The $\varepsilon_{\text{Nd}}(\text{t})$ values are also

similar to those of the S-type granites of the Lachlan Fold Belt (LFB) and Ordovician sedimentary rocks in eastern Australia (e.g., Healy et al., 2004). Group 2 samples have slightly lower initial $^{87}\text{Sr}/^{86}\text{Sr}$ ratios (0.7073-0.7278) and relatively higher $\varepsilon_{\text{Nd}}(t)$ values (-8.3~-11.0) than those of Group 1 samples, mostly falling in the I- and S-type granite fields from the Lachlan Fold Belt (e.g., Healy et al., 2004). The Nd model ages range from 2.92 Ga to 1.84 Ga and 2.88 Ga to 1.51 Ga for Group 1 and 2 samples, respectively (Table 3).

6. Discussion

6.1. Petrogenetic constraints of late Triassic granites in NW Thailand

Group 1 samples generally show negative correlations between SiO_2 and FeOt , MgO , Al_2O_3 , CaO , P_2O_5 , TiO_2 , Sr , Ba and Eu^* . These signatures, along with variation trends between Sr and Ba and Rb and depletion in Eu , P and Ti in Fig. 8a-b, suggest the removal of plagioclase, K-feldspar, biotite, Fe-Ti oxides and apatite. Group 1 samples show $\text{K}_2\text{O}>\text{Na}_2\text{O}$, suggestive of the K-rich rather than Na-rich magma, against the petrogenesis of the aluminous-poor mafic magma crystallization.

Available petrological and geochemical data indicate that large-volume peraluminous granites originate from continental crustal materials involving metapelites, greywackes and metaigneous rocks (e.g., Miller 1985; Beard et al., 1993; Douce and Beard, 1995; Sylvester, 1998; Clemens, 2003; Wang et al., 2007, 2013, 2014). Group 1 and 2 samples exhibit variable K_2O (3.2-10.2 wt%), Rb/Sr (0.4-5.3), Sm/Nd (0.18-0.25), Cr/Th (0.3-4.2), Ra/Ba , $\text{CaO}/\text{Al}_2\text{O}_3$ and $\text{Al}_2\text{O}_3/\text{TiO}_2$ ratios,

generally higher than those of the sole pelite-derived melt and Himalaya strongly peraluminous granite, and bridge between the pelite- and metabasite-derived magmas in Fig. 10a-b (e.g., Douce and Beard, 1995; Springer and Seck, 1997; Sylvester, 1998; Zhang et al., 1999; Altherr et al., 2000). In comparison with Group 1 samples, Group 2 samples have relatively higher CaO/Na₂O and lower Rb/Sr ratios at comparable Al₂O₃/TiO₂ and Rb/Ba, respectively. In Figure 10c-d, Group 1 samples show two distinct trends with one having low CaO+MgO+FeOt+TiO₂ and Al₂O₃+MgO+FeOt+TiO₂ but sharply increasing CaO/(MgO+FeOt+TiO₂) and Al₂O₃/(MgO+FeOt+TiO₂) ratios, while the other shows the opposite trends, suggesting a mixed source involving metapelite and metabasite components (e.g., Chappell and White, 1992; Sylvester, 1998; Anthony, 2005; Wang et al., 2013). However, Group 2 samples show low CaO/(MgO+FeOt+TiO₂) and Al₂O₃/(MgO+FeOt+TiO₂) ratios, falling into the field of greywacke and metabasite derivations in Fig. 10c-d (e.g., Douce and Beard, 1995; Sylvester, 1998; Clemens, 2003). In the plot of ϵ Nd(t) and A/CNK (Fig. 11a), it is shown for a hyperbolic correlation. Such binary hybridization for the Group 1 and Group 2 sources are further supported by the linear correlations in Figures 11b-c. As shown in Figure 9, the Sr-Nd isotopic compositions for both groups are distinct from those of the Gangdese I-type and Sibumasu Paleozoic granites (e.g., Xu et al., 2008, 2012; Ma et al., 2014). Instead, such isotopic variations dominantly fall into the ranges of the Kwangolian and Indosinian granites in the SCB, Lachlan S-type granites and Australia Ordovician sedimentary rocks, which are interpreted as the derivation of metapelite or the mixing source composed of metapelite and metabasite (e.g., Li and

McCulloch, 1996; Wang et al., 2007, 2013; Shen et al., 2009; Peng et al., 2013).

Zircon Hf-O isotopic compositions are considered to be useful tools for probing the granitic source (e.g. Griffin et al. 2002; Valley et al., 2005; Yang et al. 2007; Kemp et al. 2007; Bolhar et al. 2008). The $\delta^{18}\text{O}$ values for mantle-derived zircon have a narrow range of $5.3 \pm 0.6\text{\textperthousand}$ (Valley, 2003; Valley et al., 2005) and increase with the involvement of the supracrustal materials (e.g. Li et al., 2009; Eiler, 2001). The Triassic crystallization zircons from Group 1 samples give the $\epsilon\text{Hf(t)}$ values ranging from -5.4 to -18.2 with the peaks at -11.2 and -13.7 (Fig. 12a). The corresponding Hf model ages vary from 1.62 Ga to 2.40 Ga with the peaks at 1.9 Ga and 2.1 Ga (Fig. 12b). The zircon $\delta^{18}\text{O}$ values of $>7.5\text{\textperthousand}$ are commonly attributed to melting or assimilation of a supracrustal source, e.g., sedimentary rocks or altered volcanic rocks (e.g., Peck et al. 2004; Valley et al., 2005; Fu et al., 2016; Jiao et al., 2015). The $\delta^{18}\text{O}$ values of the Triassic magmatic zircons in Group 1 samples range from +7.95 to +9.94 with the peak at +9.1 (Fig. 12c), similar to those of Hunan Triassic granites related to a mixed metapelite and metavolcanic source (Wang et al., 2007), but lower than those of the Triassic Darongshan S-type granites that are commonly interpreted as the derivation of the sole supracrustal source (Fig. 13). In addition, the inherited zircons with U-Pb ages of 1411-422 Ma give the $\delta^{18}\text{O}$ values of 8.1-9.4‰ (peak at 8.7‰) and variable $\epsilon\text{Hf(t)}$ values of -11.0-+5.4 that plotted along the evolved array (Fig. 12a-b), indicating that these inherited grains also experienced surface weathering process. As a result, the Sr-Nd-Hf-O isotopic characteristics, along with the A/CNK ratios of 0.95-1.43 and the presence of the Proterozoic to early Paleozoic inherited

zircons for Group 1 samples (Figs. 9-13), indicate the derivation of the Paleozoic supracrustal materials involving metapelitic and metavolcanic rocks that have previously experienced surface weathering.

The Group 2 samples have the A/CNK ratios of 0.91-1.08, with a geochemical affinity to I-type granites. They exhibit relatively higher $\epsilon_{\text{Nd}}(t)$ values at comparable $^{87}\text{Sr}/^{86}\text{Sr}(t)$ and A/CNK than Group 1 samples (Fig. 9 and 11a). The zircon in-situ $\epsilon_{\text{Hf}}(t)$ values for Group 2 samples range from -11.1 to +4.80 (peaks at -10 and +3.0), higher than those of Group 1 samples, and T_{DM} values from 0.96 Ga to 1.95 Ga (peaks at 1.1 Ga and 1.9 Ga), younger than those of Group 1 samples (Fig. 12a-b). Such signatures, together with the elemental characteristics in Figure 11b-c, suggest a binary mixing source. The late Triassic grains from Group 2 samples have $\delta^{18}\text{O}$ values of +4.95~+7.98 (peaks at +5.7 and +7.2), which are significantly lower than Group 1 samples (Fig. 12c). Such $\delta^{18}\text{O}$ values plot along the array of mantle- and crust-derived zircons (Figs. 12-13), generally suggesting the absence of water-rock interaction (e.g., Valley, 2003; Valley et al., 2005). Their positive $\epsilon_{\text{Hf}}(t)$ values, young T_{DM} and low $\delta^{18}\text{O}$ values, along with the absence of ancient inherited zircons, indicate the involvement of a newly underplated mafic component for the Group 2 source (Fig. 12). This is further evidenced by late Triassic I-type rhyolite (229 Ma) along the Chiang Khong-Lampang -Tak volcanic zone of Eastern Province that originated from juvenile mafic crust, which is characterized by low TiO_2 , MgO and $\delta^{18}\text{O}$ (5.3-5.9 ‰) and high $\epsilon_{\text{Nd}}(t)$ values (+1.1-+1.3) and $\epsilon_{\text{Hf}}(t)$ (+4~+12) (Qian et al., 2016). Taking into account the negative $\epsilon_{\text{Nd}}(t)$ values (-8.3 to -11.0), along with the negative $\epsilon_{\text{Hf}}(t)$ and

relatively high $\delta^{18}\text{O}$ values for zircons from Group 2 samples (Figs. 12-13), it is inferred that the Group 2 source contains an "older" component. This is further supported by the presence of the angular to rounded amphibolite and gneissic enclaves in the Tak granitic pluton. In summary, Group 2 samples might originate from a hybridized source of a newly underplated mafic with an ancient metamorphic component.

6.2. Temporal pattern of the Paleotethyan evolution in NW Thailand

Our data show that the granitic gneiss in the Inthanon zone (Central Province) give weighted mean ages of 219 ± 2 Ma (TG-5A), 200 ± 2 Ma (TG-6A), 222 ± 3 Ma (TG-30B₁), 212 ± 3 Ma (TG-52A) and 207 ± 2 Ma (TG-53A₂). The massive granites in the Inthanon zone (Central Province) yield weighted mean ages of 226 ± 3 Ma (TL-26A), 220 ± 1 Ma (TG-11A), 210 ± 1 Ma (TG-42A) and 223 ± 2 Ma (TG-16B₁). In addition, the massive granite in the Sukhothai zone (Eastern Province) have weighted mean ages of 220 ± 3 Ma (TG-8A), 216 ± 2 Ma (TL-13A₁), 214 ± 1 Ma (TG-26C) and 224 ± 2 Ma (TG-27A). Khositanont et al. (2007), Zaw and Meffre (2007) and Gardiner et al. (2015) also obtained the LA-ICP-MS and SIMS zircon U-Pb ages in the range of 229-215 Ma from the granites at Mae Long and Mae Sariang (Inthanon zone) and Mae Khaem, Mae Mok, Denchai and Tak (Sukhothai zone). Such data reveal the development of the late Triassic (230-200 Ma) granites in NW Thailand, synchronous with the late Triassic (232-220 Ma) volcanic rocks in the Sukhothai zone (e.g., Qian et al., 2015a; Srichan, et al., 2009; Barr, et al., 2006).

In the Inthanon zone, late Paleozoic pelagic radiolarian cherts, limestones,

mudstones, turbidites and basaltic rocks are widespread (e.g., Fang et al., 1994; Feng et al., 2001; Ueno and Hisada, 2001; Feng, 2002; Feng et al., 2004, 2008; Wakita and Metcalfe, 2005; Hara et al., 2009; Ridd et al., 2011). Wang et al. (2016) recently reported that basalts capped by shallow-marine carbonate build-ups in the zone are characterized by high-Fe OIB-type tholeiitic basalts and erupted at 282.3 ± 1.4 Ma, which are interpreted to have formed in an oceanic, seamount environment. Kamvong and Zaw (2009) and Salam et al. (2014) identified the early Triassic (243-244 Ma) quartz monzonite porphyry and granodiorite in the Sukhothai zone most likely forming in a supra-subduction zone. Feng et al. (2002, 2004) and Ueno (1999, 2003) proposed the drowning and accretion of Paleotethyan seamount and the closure of Paleotethyan ocean in NW Thailand occurred in the Triassic at Olenekian (~247 Ma and Ladinian (~237 Ma), respectively, based on the foraminiferal assemblage in Doi Chiang Dao limestone and radiolarian assemblage in Fang chert (Ueno and Hisada, 2001). Such observations favor the Paleotethyan Ocean closing by the middle Triassic (~237 Ma) rather than the late Triassic or later as proposed by Barr et al. (2000, 2006).

In Sukhothai zone, the Chiang Khong-Lampang volcanic zone composed of the andesite, rhyolite, dacite and tuff. These volcanic rocks give two age clusters of 242-237 Ma and 232-220 Ma, which are interpreted as the arc (or syncollisional) and post-collisional products, respectively (e.g., Barr et al. 2000, 2006; Srichan et al. 2009; Qian et al. 2013, 2015a). These data, along with the geological observation that the volcanic sequence is uncomfortably bounded by the Permian–lowest Triassic

sequence and the upper Triassic-lower Jurassic molasses (e.g., Barr and Macdonald, 1991; Hara et al., 2009; Ridd et al., 2011), define that the collision of the Sibumasu with Indochina blocks initiated in the early Triassic and ended by the latest Triassic. In monzonitic granite sample TL-13A₁, the inherited middle Triassic grains are ca. 237 Ma, ~20 Ma older than its emplacement age (216 Ma). The granitic gneiss enclave of TG-16A₂ is dated at 237 Ma, 14 Ma older than its massive hosted granite (223 Ma) for TG-16B₁. The 15-20 Ma time-gap between the inherited and crystallization grains is consistent with that between the syn- and post-collisional magmatism found in many belts worldwide (e.g., Liégeois, 1998; Coulon et al., 2002; Cvetković et al., 2004; Wang et al., 2010). Therefore, these data synthetically allow a possibility of proposing a switch from the subduction of Paleotethyan Ocean to the collision of the Sibumasu with Indochina blocks at ~237 Ma, and syn- and post-collisional orogenic events at ~237-230 Ma and ~200-230 Ma, respectively. As a result, Group 1 and 2 samples in the Inthanon and Sukhothai zones can be interpreted as the post-collisional magma.

6.3. Petrogenetic mechanism of late Triassic granites in NW Thailand

As mentioned above, Group 1 samples from the Inthanon zone originated from a metapelite source hybridized with metavolcanic rocks having experienced surface weathering. Group 2 granites in the Sukhothai zone were derived from the mixed source with the involvement of juvenile component (Figs. 9 and 13). Group 1 and 2 samples have generally similar Sr-Nd-Hf isotopic compositions with the Indosinian and Kwangian granites in the eastern SCB and the Triassic Lincang granites in SW

Yunnan, but distinct from the granites in the Late Mesozoic Gangdese granites and the Paleozoic Sibumasu granites (Fig. 9). This suggests that the sources for the two groups have an affinity to the Indochina and Yangtze blocks rather than the Sibumasu block. In addition, the Group 1 rocks from the Inthanon zone contain abundant early Paleozoic-Achean inherited grains (2545-420 Ma). These data, together with the high zircon in-situ $\delta^{18}\text{O}$ values, suggest the provenance of the Group 1 from early Paleozoic supracrustal rocks. Taking into account the spatial pattern of the Sibumasu and Indochina block and the Inthanon and Sukhothai zones (Figs. 1-3 and 14a) and late Paleozoic ocean rock-association in the Inthanon zone, it is concluded that the Group 1 supracrustal rocks are from the early Paleozoic package of the Sukhothai zone or the Indochina block to its east. The early Paleozoic detritus were transported southerly/westerly and deposited in the Inthanon zone to west of the Chiang Rai Fault, and were incorporated into a growing accretionary prism associated with subduction of the Paleotethys ocean beneath the Sukhothai zone. Easterly subduction beneath the Sukhothai zone induced partial melting of the mantle wedge to generate mafic magma which was underplated at the base of the zone and mixed with the ancient materials to build the Group 2 source. In the Khun Tan pluton for Group 1, the 237 Ma granitic gneiss enclave (TG-16A₂) and its 223 Ma hosted massive granite (TG-16B₁) bear the same zircon Hf-O isotopic compositions. In TL-13A₁ monzonitic granite of Group 2, the inherited middle Triassic grains (237 Ma) have similar $\epsilon_{\text{Hf}}(t)$, $\delta^{18}\text{O}$ and T_{DM} values to those with the late Triassic crystallization age of 216 Ma. This suggests the Group 1 and 2 sources having been built before the initial collision of the Sibumasu with

Indochina blocks (~237 Ma).

The syn-collisional crustal thickening and subsequent post-collisional collapse are the potential mechanisms governing the generation of the peraluminous felsic magma. As mentioned above, syn- and post-collisional orogenic events in NW Thailand occurred at ~237-230 Ma and ~230-200 Ma, respectively. Integrating available data, the following tectonic model of the Paleotethyan evolution in NW Thailand is proposed. (a) At Permian-early Triassic period (prior to 237 Ma), the Paleotethyan ocean plate was subducted easterly beneath the Sukhothai zone or the Indochina block to result into underplating of mantle-derived magma and mix with ancient materials for generating Group 1 plutons. At the same time, the sedimentary detritus is transported westerly transported into the Inthanon accretionary zone (Fig. 14b). (b) During the early-middle Triassic (~237-230 Ma), the collision of the Indochina and Sibumasu blocks induced thickening of the accretionary sedimentary rocks in the Inthanon zone and the overthrusting of the Sukhothai and Indochina sheets (Fig. 14c). Radioactive heating and shearing heating at this time (England and Thompson, 1984; Stevens and Clemens, 1993; Wang et al., 2002; Whalen et al., 2006; Peng et al., 2013) might promote the generation of a small-proportional migmatite, gneiss and its equivalents (e.g., Dewey 1982), as marked by the 237 Ma granitic gneissic enclave in the Khun Tan pluton. (c) During the period ~230-200 Ma, the gravitational collapse of the organic belt in response to the thermo-mechanical erosion (Fig. 14d) promotes the increasing thermal gradient for inducing extensive magma generation and the emplacement of the plutons, resembling those proposed for the

European Alps, Caledonides and Lachlan Fold Belt (e.g., Altherr et al., 1995; Searle et al., 1997; Sylvester, 1998; Villaseca et al., 1998). Such a process facilitates the anatexis of the metasedimentary source in the Inthanon zone to produce the Group 1 granite, and the dehydrated melting of the newly hybridized source in the Sukhothai zone to generate the Group 2 magma.

6.4. Linkage with the Triassic Lincang granite in SW Yunnan

As mentioned above, the igneous rocks in NW Thailand are mainly constituted by Triassic granite and the Chiang Khong–Lampang volcanic zone. A similar relationship occurs in SW Yunnan to the east of the Changning-Menglian suture zone, which consists of the Lincang granite and the Lancangjiang volcanic zone. Question remains as to whether the Triassic igneous rocks in NW Thailand are temporally and spatially related to those in SW Yunnan. The Lincang granite formed at ~230-220 Ma (Wang et al., 2010; Peng et al., 2013), synchronous with the granites (230-200 Ma) in the Inthanon and Sukhothai zones, both of which are interpreted as the post-collisional products. Additionally, the Kyaing Tong granite in NW Laos bridging between NW Thailand and SW Yunnan is dated at 220-214 Ma (Than Htun et al., 2014; Gardiner et al., 2015). Thus, the granitic rocks in NW Thailand might represent the southward extension of the Lincang granites in SW Yunnan.

The Manghuai and Xiaodingxi/Manghuihe volcanic rocks in SW Yunnan erupted at 241–231 Ma and 220-210 Ma, and are interpreted as syn- and post-collisional products, respectively (e.g., Jian et al., 2004; Peng et al., 2006; Wang et al., 2010). Similarly, the Chiang Khong–Lampang volcanic rocks in NW Thailand yield two

ages clusters of 242-237 Ma and 230-220 Ma, and show similar rock-associations to the Manghuai and Xiaodingxi/Manghuihe volcanic sequences in SW Yunnan (e.g., Qian et al., 2013, 2015; Srichan, et al., 2009; Barr, et al., 2006; Panjasawatwong, 2003; Barr and Charusiri, 2011). These data are consistent with the tectonic models invoking initial collision of the Simao and Baoshan blocks at ~242 Ma, and the syn- and post- collisional events at ~242-230 Ma and ~230-210 Ma, respectively (e.g., Peng et al., 2006, 2013; Barr et al., 2000, 2006; Wang et al., 2010; Fan et al., 2015).

In NW Thailand, the Nan suture zone, Chiang Rai Fault and Mae Yuan/Inthanon zone have all been proposed as marking the Paleotethyan suture (e.g., Bunopas, 1994; Feng, 2002; Feng et al., 2008; Ueno, 2003; Ferrari et al., 2008; Hara et al., 2009; Metcalfe, 2002; Metcalfe and Isozaki, 2009; Panjasawatwong et al. 2006; Qian et al. 2015a, 2016; Wang et al., 2016). In theory, the syn- and post-collisional granites and their equivalents should develop in the hangingwall rather than footwall of the main suture formed during ocean closure. Our Group 1 and Group 2 granites are exposed in the Inthanon and Sukhothai zones across the Chiang Rai Fault, respectively. Taking into account the well-developed late Paleozoic seamount basalt and associated deep-sea sedimentary rocks within the Inthanon zone and the discussion in Section 6.3, it is inferred that the Inthanon zone represents the main suture of the Paleotethyan Ocean in NW Thailand and the Mae Yuan fault is the western boundary of the suture zone, which extends northwards into the Changning-Menglian suture zone in SW Yunnan (Fig. 1). In fact, recent data suggest that the Nan suture, forming in late Carboniferous, represents the remnants of a back-arc basin rather than a main ocean

(Fig. 14a; e.g., Ferrari et al., 2008; Sone and Metcalfe, 2008; Barr and Charusiri, 2011; Metcalfe, 2011, 2013; Qian et al., 2014, 2016). This suture extends northwards into the similarly-aged Luang Prabang (NW Laos) and Jinghong/Ailaoshan (SW Yunnan) back-arc basins (Fig. 14a; e.g., Fan et al., 2010; Lai et al., 2014; Qian et al., 2015b). The Sukhothai zone bounded by the Chang Rai Fault and Nan suture might be considered to be a Permian-early Triassic continental arc with an affinity to the Indochina Block, representing the southward extension of the Lincang arc in SW Yunnan (Figs. 1 and 14a; e.g., Barr and Macdonald, 1991; Hennig et al., 2009; Wang et al., 2010; Peng et al., 2013). These data synthetically suggest that the Paleotethyan pattern is spatially characterized by the Inthanon suture zone, Sukhothai arc and Nan back-arc basin from west to east, corresponding to the Changning-Menglian suture zone, Lincang arc and the Jinghong back-arc basin in SW Yunnan (Figs. 1 and 14a; e.g., Barr and Macdonald, 1991; Hennig et al., 2009; Hara et al., 2009; Wang et al., 2010; Peng et al., 2008, 2013; Fan et al., 2015). As a result, it is generally identical for the temporal-spatial pattern of Paleotethyan evolution in NW Thailand and SW Yunnan.

Acknowledgements: We would like to thank L-Y Ma and X-P Xia for their help during fieldwork and zircon U-Pb analyses. We also thank Prof. S-L Chung for his helpful editorial suggestion and Drs. X-R Zhang and S Li for their thorough, critical and constructive comments. This study was jointly funded by the National Science Foundation of China (41190073), National Basic Research Program of China (2014CB440901 and 2016YFC0600303) and the Fundamental Research Funds for the

Central Universities to SYSU.

References

- Altherr, R., Lugovic, B., Meyer, H.P., Majer, V., 1995. Early Miocene post-collisional calc-alkaline magmatism along the easternmost segment of the periadriatic fault system (Slovenia and Croatia). *Mineralogy and Petrology* 54(3-4), 225-247.
- Altherr, R., Holl, A., Hegner, E., Langer, C., Kreuzer, H., 2000. High-potassium, calc-alkaline I-type plutonism in the European Variscides: Northern Vosges (France) and Northern Schwarzwald (Germany). *Lithos* 50(1), 51-73.
- Anthony, E.Y., 2005. Source regions of granites and their links to tectonic environment: examples from the western United States. *Lithos* 80(80), 61-74.
- Barr, S.M., Macdonald A.S., 1991. Toward a Late Paleozoic-Early Mesozoic tectonic model for Thailand. *Journal of Thailand Geosciences* 1, 11–22.
- Barr, S.M., MacDonald, A.S., Ounchanum, P., Yaowanoiyothin, W., 2000. Petrochemistry, U-Pb (zircon) age, and paleotectonic setting of the Lampang volcanic belt, Central Thailand. *Journal of the Geological Society* 157, 553–563.
- Barr, S.M., Macdonald, A.S., Ounchanum, P., Hamilton, M.A., 2006. Age, tectonic setting and regional implications of the Chiang Khong volcanic suite, Northern Thailand. *Journal of the Geological Society* 163, 1037–1046.
- Barr, S.M., Charusiri, P., 2011. Volcanic rocks. In: Ridd, M.F., Barber, A.J., Crow, M.J. (eds.), *The Geology of Thailand*. Geological Society, London, p 415–439.
- Beard, J. S., Abirz. R.J, Lofgren, G.E., 1993. Experimental melting of crustal xenoliths from Kilbourne Hole, New Mexico and implications for the contamination and genesis of magmas. *Aids Research & Human Retroviruses* 115(1), 88-102.
- Bolhar, R., Weaver, S. D., Whitehouse, M. J., Palin, J. M., Woodhead, J. D., Cole, J. W., 2008. Sources and evolution of arc magmas inferred from coupled O and Hf isotope systematics of plutonic zircons from the Cretaceous Separation Point Suite (New Zealand). *Earth Planetary Science Letters* 268(s 3–4), 312-324.
- Bonin, B., 2004. Do coeval mafic and felsic magmas in post-collisional to within-plate

- regimes necessarily imply two contrasting, mantle and crustal, sources? A review. *Lithos* 78, 1–24.
- Bonin, B., 2007. A-type granites and related rocks: evolution of a concept, problems and prospects. *Lithos* 97, 1–29.
- Bullard, E., Smith, A. G., 1965. The fit of the continents around the atlantic. *Philosophical Transactions of the Royal Society A Mathematical Physical & Engineering Sciences* 258(258), 41-51.
- Caridroit, M., 1993. Permian radiolaria from NW Thailand. In: Thana-Suthipitak. T. (ed.) *Proceedings of the international symposium on biostratigraphy of Mainland Southeast Asia Facies and Paleontology 1*, Chiang Mai, Thailand 83–96.
- Cawood, P.A., Wang, Y.J., Xu, Y.J., Zhao, G.C., 2013. Locating South China in Rodinia and Gondwana: a fragment of greater India lithosphere? *Geology* 41(8), 903-906.
- Chappell, B.W., White, A.J.R., 1974. Two contrasting granite types. *Pacific Geology* 8, 173–174.
- Chappell, B. W., White, A. J. R., 1992. I- and S-type granites in the Lachlan Fold Belt. *Earth and Environmental Science Transactions of the Royal Society of Edinburgh* 83(83), 1-26.
- Chappell, B.W., White, A.J.R., 2001. Two contrasting granite types: 25 years later. *Australian Journal of Earth Sciences* 48, 488–489.
- Chappell, B. W., White, A. J. R., 1992. I- and S-type granites in the Lachlan Fold Belt. *Earth and Environmental Science Transactions of the Royal Society of Edinburgh* 83(83), 1-26.
- Clemens, J.D., 2003. S-type granitic magmas-petrogenetic issues, models and evidence. *Earth-Science Reviews* 61, 1–18.
- Cobbing, E.J., Mallic, D.I.J., Pitfield, P.E.J., Teoh, L.H., 1986. The granites of the Southeast Asian tin belt. *Journal of the Geological Society* 143(3), 537–550.
- Cobbing, E.J., 1990. A comparison of granites and their tectonic settings from the South American Andes and the Southeast Asian tin belt. *Geological Society of America Special Papers*, 193-204.
- Cobbing, E.J., Pitfield, P.E., Darbyshire, D.P.F., Mallick, D.I.J., 1992. The granites of the Southeast Asian tin belt. *Overseas memoir of the British geological survey* 10, 1–369 Her Majesty's Sth Off, Norfolk, England.
- Coulon, C., Megartsi, M., Fourcade, S., Maury, R. C., Bellon, H., Louni-Hacini, A., Cottend,

J., Coutelé, A., Hermitte, D., 2002. Post-collisional transition from calc-alkaline to alkaline volcanism during the Neogene in Oranie (Algeria): magmatic expression of a slab breakoff. *Lithos* 62(3–4), 87–110.

Cvetković, V., Prelević, D., Downes, H., Jovanović, M., Vaselli, O., Pécsay, Z., 2004. Origin and geodynamic significance of tertiary Post-collisional basaltic magmatism in Serbia (Central Balkan Peninsula). *Lithos* 73(3–4), 161–186.

Dewey, J. F., 1982. Plate tectonics and the evolution of the British Isles. *Journal of the Geological Society of London* 139, 371–412.

Douce, A. E. P. and Beard, J. S., 1995. Dehydration-melting of biotite gneiss and quartz amphibolite from 3 to 15 kbar. *Journal of Petrology* 36(3), 707–738.

Dunning, G.R., Macdonald, A.S., Barr, S.M., 1995. Zircon and monazite U–Pb dating of the Doi Inthanon core complex, Northern Thailand: implications for extension within the Indosinian Orogen. *Tectonophysics* 251, 197–213.

Eiler, J. M., 2001. Oxygen isotope variations of basaltic lavas and upper mantle rocks. *Reviews in Mineralogy & Geochemistry* 43(1), 319–364.

England, P.C., Thompson, A.B., 1984. Pressure-temperature-time paths of regions metamorphism I. heat transfer during the evolution of regions of thickened continental crust. *Journal of Petrology* 25, 894–928.

Fan, W.M., Wang, Y.J., Zhang, A.M., Zhang, F.F., Zhang, Y.Z., 2010. Permian arc-back-arc basin development along the Ailaoshan tectonic zone: geochemical, isotopic and geochronological evidence from the Mojiang volcanic rocks, Southwest China. *Lithos* 119, 553–568.

Fan, W.M., Wang, Y.J., Zhang, Y.H., Zhang, Y.Z., Jourdan, F., Zi, J.W., Liu, H.C., 2015. Paleotethyan subduction process revealed from Triassic blueschists in the Lancang tectonic belt of Southwest China. *Tectonophysics* 662, 95–108.

Fang, N.Q., Liu, B.P., Feng, Q.L., 1994. Late Paleozoic and Triassic deep-water deposits and tectonic evolution of the Palaeotethys in the Changning-Menglian and Lancangjiang belts, Southwestern Yunnan. *Journal of Southeast Asian Earth Sciences* 9(4), 363–374.

Feng, Q., Meischner, D., Rucha, I. H., Dietrich, H., Chonglakmani, C., 2001. Correlation of tectono-stratigraphic units in Northern Thailand with those of Western Yunnan (China). *Journal of China University of Geosciences*, 12(3).

- Feng, Q.L., 2002. Stratigraphy of volcanic rocks in the Changning-Menglian Belt in Southwestern Yunnan, China. *Journal of Asian Earth Sciences* 20(6), 657–664.
- Feng, Q.L., Chongpan, C., Dietrich, H., Ingavat-Helmcke, R., 2004. Long-lived Paleotethyan pelagic remnant inside Shan-Thai Block: evidence from radiolarian biostratigraphy. *Science in China Series D: Earth Sciences* 47(12), 1113–1119.
- Feng, Q.L., Yang, W.Q., Shen, S.Y., Chonglakmani, C., Malila, K., 2008. The Permian seamount stratigraphic sequence in Chiang Mai, North Thailand and its tectogeographic significance. *Science in China Series D: Earth Sciences* 51(2), 1768–1775.
- Ferrari, O.M., Hochard, C., Stampfli, G.M., 2008. An alternative plate tectonic model for the Paleozoic–Early Mesozoic Paleotethyan evolution of Southeast Asia (Northern Thailand–Burma). *Tectonophysics* 451, 346–365.
- Fontaine, H., 2002. Permian of Southeast Asia: an overview. *Journal of Asian Earth Sciences* 20(6), 567–588.
- Gardiner, N.J., Searle, M.P., Morley, C.K., Whitehouse, M.P., Spencer, C.J., Robb, L.J., 2015. The closure of Palaeotethys in Eastern Myanmar and Northern Thailand: new insights from zircon U–Pb and Hf isotope data. *Gondwana Research* doi:10.1016/j.gr.2015.03.001
- Griffin, W.L., Wang, X., Jackson, S.E., Pearson, N.J., O'Reilly, S.Y., Xu, X., et al., 2002. Zircon chemistry and magma mixing, SE China: In-situ analysis of Hf isotopes, Tonglu and Pingtan igneous complexes. *Lithos* 61(3), 237–269.
- Hada, S., Bunopas, S., Ishii, K., Yoshikura, S., 1997. Rift-drift history and the amalgamation of Shan-Thai and Indochina/East Malaya Blocks. In: Dheeradilok P, Hinthon C, Chaodumrong P, Putthapiban P, Tansathien W, Utha-Aroon C, Sattyarak N, Nuchanong T, and Techawan S., eds. *Proceedings of the International Conference on Stratigraphy and Tectonic Evolution of Southeast Asia and the South Pacific*. Bangkok, Thailand 273–286.
- Hara, H., Wakita, K., Ueno, K., Kamata, Y., Hisada, K.I., Charusiri, P., Charoentitirat, T., Chaodumrong, P., 2009. Nature of accretion related to Paleotethys subduction recorded in Northern Thailand: constraints from mélange kinematics and illite crystallinity. *Gondwana Research* 16, 310–320.
- Hennig, D., Lehmann, B., Frei, D., Belyatsky, B., Zhao, X.F., Cabral, A.R., Zeng, P.S., Zhou, M.F., Schmidt, K., 2009. Early Permian seafloor to continental arc magmatism in the eastern

Paleo-Tethys: U–Pb age and Nd–Sr isotope data from the Southern Lancangjiang zone, Yunnan, China. *Lithos* 113, 408–422.

Healy, B., Collins, W. J., Richards, S.W., 2004. A hybrid origin for Lachlan S-type granites: the Murrumbidgee batholith example. *Lithos* 78(1–2), 197–216.

Hutchison, C.S., 1975. Ophiolites in Southeast Asia. *Geological Society of America Bulletin*. 86, 797–806.

Hutchison, Mark, T., Nielsen, Josefine, L., Bernstein, Stefan, 2007. Review of survey activities 2006: P–T history of kimberlite-hosted garnet lherzolites from South-west Greenland. *Geological Survey of Denmark & Greenland Bulletin*, 13(13), 45–48.

Kamvong, T., Zaw, K., 2009. The origin and evolution of skarn-forming fluids from the Phu Lon deposit, Northern Loei Fold Belt, Thailand: evidence from fluid inclusion and sulfur isotope studies. *Journal of Asian Earth Sciences* 34(5), 624–633.

Kemp, A.I.S., Hawkesworth, C.J., Foster, G.L., Paterson, B.A., Woodhead, J.D., Hergt, J.M., Gray, C.M., 2007. Magmatic and crustal differentiation history of granitic rocks from Hf–O isotopes in zircon. *Science* 315, 980–983.

Khositanont, S., Ounchanum, P., Panjasawatwong, Y., Thanasuthipitak, T., Khin Zaw, Meffre, S., 2007. U-Pb Zircon Ages and Geochemical Characteristics of Lapang-Phrae Granites; Implications for Plate Tectonic Interpretation. the Geothai'07 International Conference on Geology of Thailand: Towards Sustainable Development and Sufficiency Economy, 367–372.

Lai, C.K., Meffre, S., Crawford, A.J., Zaw, K., Halpin, J.A., Xue, C.D., Salam, A., 2014. The Central Ailaoshan ophiolite and modern analogs. *Gondwana Research* 26, 75–88.

Lepvrier, C., Van Vuong, N., Maluski, H., Truong Thi, P., Van Vu, T., 2008. Indosinian tectonics in Vietnam. *Comptes Rendus Geoscience* 340, 94–111.

Li, C., Zhai, Q.G., Xu, F., Zhu, Z.Y., 2005. Kinematics of the active North-South-trending Chazang Co-Xainza tectonic Belt, Xizang (Tibet). *Geological Review* 51(4), 353–359.

Li, X.H., Mcculloch, M.T., 1996. Secular variation in the Nd isotopic composition of Neoproterozoic sediments from the Southern margin of the Yangtze block: evidence for a Proterozoic continental collision in Southeast China. *Precambrian Research* 76(1–2), 67–76.

Li, X.H., Li, Z.X., Zhou, H.W., Liu, Y., Kinny, P.D., 2002. U–Pb zircon geochronology, geochemistry and Nd isotopic study of Neoproterozoic bimodal volcanic rocks in the Kangdian

Rift of South China: implications for the initial rifting of Rodinia. *Precambrian Research* 113(1-2), 135-154.

Li, X. H., Li, W. X., Wang, X. C., Li, Q. L., Liu, Y., Tang, G. Q., 2009. Role of mantle-derived magma in genesis of early Yanshanian granites in the Nanling range, South China: in situ, zircon Hf-O isotopic constraints. *Science in China* 52(9), 1262-1278.

Li, X.H., Li, W.X., Li, Q.L., Wang, X.C., Liu, Y., Yang, Y.H., 2010. Petrogenesis and tectonic significance of the 850 Ma Gangbian alkaline Complex in South China: evidence from in situ zircon U-Pb dating, Hf-O isotopes and whole-rock geochemistry. *Lithos* 114, 1–15.

Li, X.H., Tang, G.Q., Gong, B., Yang, Y.H., Hou, K.J., Hu, Z.C., Li, Q.L., Liu, Y., Li, W.X., 2013. Qinghu zircon: A working reference for microbeam analysis of U-Pb age and Hf and O isotopes. *Chinese Science Bulletin* 58, 4647–4654.

Liégeois, J.P., 1998. Some words on the post-collisional magmatism. *Lithos*, 45, XV-XVIII.

Ludwig, K.R., 2003. ISOPLOT 3.00: a geochronological toolkit for Microsoft Excel. Berkeley Geochronology Center, California, Berkeley.

Ma, L.Y., Wang, Y.J., Fan, W.M., Geng, H., Cai, Y.F., Zhong, H., Li, H.C., Xing, X.W., 2014. Petrogenesis of the early Eocene I-type granites in West Yingjiang (SW Yunnan) and its implication for the eastern extension of the Gangdese batholiths. *Gondwana Research* 25(1), 401-419.

Mahawat, C., Atherton, M.P., Brotherton, M.S., 1990. The Tak Batholith, Thailand: the evolution of contrasting granite types and implications for tectonic setting. *Journal of Asian Earth Sciences* 4(1), 11-27.

Martin, H., 1987. Petrogenesis of Archean trondhjemites, tonalites and granodiorites from eastern Finland: major and trace element geochemistry. *Journal of Petrology* 28, 921–953.

Metcalfe, I., 1996. Gondwanaland dispersion, Asian accretion and evolution of Eastern Tethys. *Australian Journal of Earth Science* 43(6), 605–623.

Metcalfe, I., 1998. Paleozoic and Mesozoic geological evolution of the SE Asian region: multidisciplinary constraints and implications for biogeography. *Biogeography and Geological Evolution of SE Asia* 25–41.

Metcalfe, I., 2002. Permian tectonic framework and palaeogeography of SE Asia. *Journal of Asian Earth Sciences* 20, 551–566.

- Metcalfe, I., 2006. Paleozoic and Mesozoic tectonic evolution and palaeogeography of East Asian crustal fragments: The Korean Peninsula in context. *Gondwana Research* 9, 24–46.
- Metcalfe, I., Isozaki, Y., 2009. Current perspectives on the Permian–Triassic boundary and end-Permian mass extinction: preface. *Journal of Asian Earth Sciences* 36(6), 407–412.
- Metcalfe, I., 2011. Palaeozoic–Mesozoic history of SE Asia. Geological Society, London, Special Publications 355, 7–35.
- Metcalfe, I., 2013. Gondwana dispersion and Asian accretion: Tectonic and palaeogeographic evolution of eastern Tethys. *Journal of Asian Earth Sciences* 66, 1–33.
- Metcalfe, I., Aung, K. P., 2014. Late Tournaisian conodonts from the Taungnyo group near Loi Kaw, Myanmar (Burma): implications for Shan Plateau stratigraphy and evolution of the Gondwana-derived Sibumasu terrane. *Gondwana Research* 26(26), 1159–1172.
- Miller, C.F., 1985. Are strongly peraluminous magmas derived from pelitic sedimentary sources? *Journal of Geology* 93, 673–689.
- Mo, X.X., Shen, S.Y., Zhu, Q.W., 1998. Volcanics-ophiolite and mineralization of middle and southern part in Sanjiang, Southern China. Beijing: Geological Publishing House, 1–128.
- Panjasawatwong, Y., 2003. Tectonic Setting of the Permo-Triassic Chiang Khong volcanic rocks, Northern Thailand based on petrochemical characteristics. *Gondwana Research* 6, 743–755.
- Panjasawatwong, Y., Khin, Zaw., Chantaramee, S., Limtrakun, P., Pirarai, K., 2006. Geochemistry and tectonic setting of the Central Loei volcanic rocks, Pak Chom area, Loei, Northeastern Thailand. *Journal of Asian Earth Sciences* 26, 77–90.
- Pearce, J.A., Harris, N.B.W., Tindle, A.G., 1984. Trace element discrimination diagrams for the tectonic interpretation of granitic rocks. *Journal of Petrology* 25, 956–983.
- Peng, T.P., Wang, Y.J., Fan, W.M., Liu, D.Y., Shi, Y.R., Miao, L.C., 2006. SHRIMP zircon U-Pb geochronology of early Mesozoic felsic igneous rocks from the southern Lancangjiang and its tectonic implications. *Science in China (Series D)* 49, 1032–1042.
- Peng, T.P., Wang, Y.J., Zhao, G.C., Fan, W.M., Peng, B.X., 2008. Arc-like volcanic rocks from the southern Lancangjiang zone, SW China: geochronological and geochemical constraints on their petrogenesis and tectonic implications. *Lithos* 102, 358–373.
- Peng, T.P., Wilde, S.A., Wang, Y.J., Fan, W.M., Peng, B.X., 2013. Mid-Triassic felsic igneous rocks from the southern Lancangjiang Zone, SW China: Petrogenesis and implications for the

evolution of Paleotethys. *Lithos* 168–169, 15–32.

Peng, T.P., Zhao, G.C., Fan, W.M., Peng, B.X., Mao, Y.S., 2014. Zircon geochronology and Hf isotopes of Mesozoic intrusive rocks from the Yidun Terrane, Eastern Tibetan Plateau: petrogenesis and their bearings with Cu mineralization. *Journal of Asian Earth Sciences* 80(2), 18-33.

Qian, X., Feng, Q.L., Chonglakmani, C., Monjai, D., 2013. Geochemical and geochronological constrains on the Chiang Khong volcanic rocks (Northwestern Thailand) and its tectonic implications. *Frontiers of Earth Science* 7, 508–521.

Qian, X., Feng, Q.L., Yang, W.Q., Wang, Y.J., Chonglakmani, C., Monjai, D., 2015a. Arc-like volcanic rocks in NW Laos: Geochronological and geochemical constraints and their tectonic implications. *Journal of Asian Earth Sciences* 98, 342–357.

Qian, X., Feng, Q.L., Yang, W.Q., Wang, Y.J., Chonglakmani, C., Monjai, D., 2015b. Geochronological and geochemical constraints on the mafic rocks along the luang prabang zone: carboniferous back-arc setting in Northwest Laos. *Lithos* 245, 60-75.

Qian, X., Wang, Y.J., Feng, Q.L., Zi, J.W., Zhang, Y.Z., Chonglakmani, C., 2016. Petrogenesis and tectonic implication of the Late Triassic post-collisional volcanic rocks in Chiang Khong, NW Thailand. *Lithos* 418–431.

Ridd, M.F., Barber, A.J., Crow, M.J., 2011. The geology of Thailand. Geological Society, London pp.615.

Ridd, M. F., 2015. East flank of the Sibumasu block in NW Thailand and Myanmar and its possible Northward continuation into Yunnan: a review and suggested tectonostratigraphic interpretation. *Journal of Asian Earth Sciences* 104, 160-174.

Salam, A., Zaw, K., Meffre, S., Mcphie, J., Lai, C. K., 2014. Geochemistry and geochronology of the Chatree epithermal gold–silver deposit: implications for the tectonic setting of the Loei Fold Belt, central Thailand. *Gondwana Research* 26(1), 198–217.

Searle, M.P., Parrish, R.R., Hodges, K.V., Hurford, A., Ayres, M.W., Whitehouse, M.J., 1997. Shisha Pangma leucogranite, south Tibetan Himalaya: field relations, geochemistry, age, origin, and emplacement. *Journal of Geology* 105, 295–317.

Searle, M. P., 2011. Alkaline peridotite, pyroxenite, and gabbroic intrusions in the Oman Mountains, Arabia. *Canadian Journal of Earth Sciences* 21(21), 396-406.

- Sengör C, A.M., 1976. Collision of irregular continental margins: implications for foreland deformation of alpine-type orogens. *Geology* 4(12), 779–782.
- Sengör, A.M.C., Hsü, K.J., 1984. The Cimmerides of eastern Asia: history of the eastern end of Paleo-Tethys. *Mémoires de la Société Géologique de France* 147, 139–167.
- Sevastjanova, I., Clements, B., Hall, R., Belousova, E.A., Griffin, W.F., Pearson, N., 2011. Granitic magmatism, basement ages, and provenance indicators in the Malay Peninsula: insights from detrital zircon U–Pb and Hf-isotope data. *Gondwana Research* 19, 1024–1039.
- Shen, W.Z., Ling, H.F., Shu, L.S., Zhang, F.R., Xiang, L., 2009. Sm–Nd isotopic compositions of Cambrian-Ordovician strata at the Jinggangshan area in Jiangxi Province: tectonic implications. *Chinese Science Bulletin* 54(10), 1750–1758.
- Sone, M., Metcalfe, I., 2008. Parallel Tethyan sutures in mainland Southeast Asia: new insights for Paleo-Tethys closure and implications for the Indosinian orogeny. *Geoscience* 340, 166–179.
- Springer, W., Seck, H.A., 1997. Partial fusion of basic granulites at 5 to 15 kbar: implications for the origin of TTG magmas. *Contributions to Mineralogy and Petrology* 127(1), 30–45.
- Srichan, W., Crawford, A.J., Berry, R.F., 2009. Geochemistry and geochronology of Late Triassic volcanic rocks in the Chiang Khong region, Northern Thailand. *Island Arc* 32–51.
- Stevens, G., Clemens, J.D., 1993. Fluid-absent melting and the role of fluids in the lithosphere: a slanted summary? *Chemical Geology* 108, 1–17.
- Sun, S.S., McDonough, W.F., 1989. Chemical and isotopic systematics of oceanic basalts: implications for mantle composition and processes. In: Saunders, A.D., Norry, M.J. (Eds.), *Geological Society London Special Publications* 42, 313–345.
- Sylvester, R.J., 1998. Postcollisional strongly peraluminous granites. *Lithos* 45, 29–44.
- Taylor, S.R., McLennan, S.M., 1985. The continental crust: Its composition and evolution. Oxford Press Blackwell 1–312.
- Than Htun, Somboon, K., Manaka, T., 2014. Preliminary Investigation of New Tin Deposits in Mong Ton-Mong Hsat Area, Shan State (East), Myanmar. In: Win Swe, Soe Thura Tun, Myo Thant, Khin Zaw (Eds.), *Thirteenth Regional Congress on Geology, Mineral and Energy Resources of Southeast Asia GEOSEA 2014 Abstracts*, p. 8.
- Ueno, K., 1999. Gondwana/Tethys divide in East Asia: Solution from Late Paleozoic

foraminiferal paleobiogeography. In: Ratanasthien, B., Ritb, S.L. (eds) Proceedings of the International on Shallow Tethys (ST) 5. Chiang Mai, 1–5 February 45–54.

Ueno, K., Hisada, K., 2001. The Nan-Uttaradit-Sa Kaeo Suture as a main Paleotethyan suture in Thailand: is it real? *Gondwana Research* 4, 804–806.

Ueno, K., 2003. The Permian fusulinoidean faunas of the Sibumasu and Baoshan blocks: their implications for the paleogeographic and paleoclimatologic reconstruction of the Cimmerian Continent. *Palaeogeography Palaeoclimatology Palaeoecology* 193(1), 1–24.

Valley, J. W., 2003. Oxygen isotopes in zircon. *Reviews in Mineralogy & Geochemistry*, 53(1).

Valley, J.W., Lackey, J.S., Cavosie, A.J., Clechenko, C.C., Spicuzza, M.J., Basei, M.A.S., Bindeman, I.N., Ferreira, V.P., Sial, A.N., King, E.M., Peck, W.H., Sinha, A.K., Wei, C.S., 2005. 4.4 billion years of crustal maturation: oxygen isotope ratios of magmatic zircon. *Contributions to Mineralogy and Petrology* 150, 561–580.

Villaseca, C., Barbero, L., Rogers, G., 1998. Crustal origin of Hercynian peraluminous granitic batholiths of central Spain: petrological, geochemical and isotopic (Sr, Nd) constraints. *Lithos* 43, 55–79.

Wakita, K., Metcalfe, I., 2005. Ocean plate stratigraphy in East and Southeast Asia. *Journal of Asian Earth Sciences* 24, 679–702.

Wang, Y.J., Fan, W.M., Guo, F., 2002. K-Ar dating of late Mesozoic volcanism and geochemistry of volcanic gravels in the North Huaiyang belt, Dabie Orogen: constraints on the stratigraphic framework and exhumation of the Northern Dabie orthogneiss complex. *Chinese Science Bulletin* 47(20), 1688-1695.

Wang, Y.J., Fan, W.M., Sun, M., Liang, X.Q., Zhang, Y.H., Peng, T.P., 2007. Geochronological, geochemical and geothermal constraints on petrogenesis of the Indosinian peraluminous granites in the South China Block: A case study in the Hunan Province. *Lithos* 96, 475–502.

Wang, Y.J., Zhang, A.M., Fan, W.M., Peng, T.P., Zhang, F.F., Zhang, Y.H., Bi, X.W., 2010. Petrogenesis of late Triassic post-collisional basaltic rocks of the Lancangjiang tectonic zone, southwest China, and tectonic implications for the evolution of the eastern Paleotethys: geochronological and geochemical constraints. *Lithos* 120, 529–546.

- Wang, Y.J., Zhang, A.M., Cawood, P.A., Fan, W.M., Xu, J.F., Zhang, G.W., Zhang, Y.Z., 2013. Geochronological, geochemical and Nd–Hf–Os isotopic fingerprinting of an early Neoproterozoic arc–back-arc system in South China and its accretionary assembly along the margin of Rodinia. *Precambrian Research* 231, 343–371.
- Wang, Y.J., Zhang, L.M., Cawood, P.A., Ma, L.Y., Fan, W.M., Zhang, A.M., Zhang, Y.Z., Bi, X.W., 2014. Eocene supra-subduction zone mafic magmatism in the Sibumasu Block of SW Yunnan: implications for Neotethyan subduction and India–Asia collision. *Lithos* 206, 384–399.
- Wang, Y.J., Li, S.B., Ma, L.Y., Fan, W.M., Cai, Y.F., Zhang, Y.H., Zhang, F.F., 2015. Geochronological and geochemical constraints on the petrogenesis of early Eocene metagabbroic rocks in Nabang (SW Yunnan) and its implications on the neotethyan slab subduction. *Gondwana Research* 27(4), 1474–1486.
- Wang, Y.J., He, H.Y., Zhang, Y.Z., Srithai, B., Feng Q.L., Cawood, P.A., 2016. Origin of Permian OIB-like basalts with two differentiation trends in NW Thailand and implication on the Paleotethyan Ocean. *Lithos*, In press.
- Winchester, J.A., Floyd, P.A., 1977. Geochemical discrimination of different magma series and their differentiation products using immobile elements. *Chemical Geology* 20(77), 325–343.
- Whalen, J.B., Currie, K.L., Chappell, W.B., 1987. A-type granites: geochemical characteristics, discrimination and petrogenesis. *Contributions to Mineralogy & Petrology* 95(4), 407–419.
- Whalen, J. B., Mcnicoll, V. J., Staal, C. R. V., Lissenberg, C. J., Longstaffe, F. J., Jenner, G. A., Breeman, O., 2006. Spatial, temporal and geochemical characteristics of Silurian collision-zone magmatism, Newfoundland Appalachians: an example of a rapidly evolving magmatic system related to slab break-off. *Lithos* 89(3), 377–404.
- Wongwanich, T., Boucot, A.J., 2011. Devonian. In: Ridd, M.F., Barber, A.J., Crow, M.J., (Eds.), *The Geology of Thailand*. Geological Society, London, pp. 71–136.
- Wu, F., Yang, Y.H., Xie, L.W., Yang, J.H., Xu, P., 2006. Hf isotopic compositions of the standard zircons and baddeleyites used in U–Pb geochronology. *Chemical Geology* 234(1–2), 105–126.
- Xu, Y.G., Yang, Q.J., Jan, J.B., Luo, Z.Y., Huang, X.L., Shi, Y.-R., 2012. Temporal-spatial distribution and tectonic implications of the batholiths in the Gaoligong-Tengliang-Yingjiang area, western Yunnan: constraints from zircon U – Pb ages and Hf isotopes. *Journal of Asian Earth Sciences*

Sciences 53, 151 – 175.

Yang, J.H., Wu, F.Y., Chung, S.L., Wilde, S.A., Chu, M.F., 2006. A hybrid origin for the Qianan A-type granite, Northeast China: geochemical and Sr–Nd–Hf isotopic evidence. *Lithos* 89, 89–106.

Zhang, R.Y., Lo, C.H., Li, X.H., Chung, S.L., Anh, T.T., Tri, T.V., 2014. U–Pb dating and tectonic implication of ophiolite and metabasite from the Song Ma suture zone, Northern Vietnam. *American Journal of Science* 314, 649–678.

Zhong, D.L., 1998. The Paleotethys orogenic belt in west of Sichuan and Yunnan. Science Publishing House, Beijing, pp. 1–230.

Zaw, K., Meffre, S. and higher degree students, 2007. Metallogenic relations and deposit scale studies, final report. Geochronology, Metallogenesis and Deposit Styles of Loei Fold Belt in Thailand and Laos PDR. ARC Linkage Project, CODES with Industry Partners. University of Tasmania, Hobart.

Figure Captions

Fig. 1. Tectonic sketch map of SE Asia showing major tectonic boundaries (modified after Sone and Metcalfe, 2008; Peng et al., 2013; Fan et al., 2015). S. Z. means suture zone. Figs. 2 and 3 are marked by the dotted box.

Fig. 2. (a) Tectonic subdivision in NW Thailand showing the Sibumasu block, Inthanon zone, Sukhothai zone/arc and Indochina block, separated by the Nan-Uttaradit zone, Chiang Rai Fault and Mae Yuam Fault from west to east, respectively. (b) Distribution of granites in NW Thailand showing Eastern, Central and Western Granite Provinces (revised from Cobbing, 1990; Ridd et al., 2011).

Fig. 3. Geological map in NW Thailand showing sampling locations and dating results. The labeled zircon U-Pb ages are from this study, Dunning et al. (1995); Barr et al. (2000, 2006); Srichan et al. (2009); Khositanont et al. (2007); Searle (2011); Zaw et al. (2007); Khositanont (2007); Qian et al. (2013, 2015a, 2016); Than Htun et al. (2014) and Gardiner et al. (2015).

Fig. 4. Micrographs of the representative samples for Group 1 samples ((a) TG-30B₁; (b) TG-53A₂; (c) TG-11A; (d) TG-40B) and Group 2 samples ((e) TL-13A₁ and (f) TG-27A) in NW Thailand.

Fig. 5. LA-ICP-MS zircon U-Pb concordia plots with insets showing the weighted mean ages for the Triassic granite from the Central (Group 1 samples) and Eastern (Group 2 samples) Province of the Inthanon and Sukhothai zones in NW Thailand, respectively. Group 1 samples: (a) TG-5A, (b) TG-6A, (c) TG-30B₁, (d) TG-52A, (e) TG-53A, (f) TL-26A, (g) TG-11A, (h) TG-42A, (i) TG-16A₂; (j) TG-16B₁; Group 2 samples: (k) TG-8A; (l) TL-13A₁; (m) TG-27A and (n) TG-26C.

Fig. 6. QAP classification of the Triassic granite for Group 1 and 2 samples from the Inthanon and Sukhothai zones in NW Thailand.

Fig. 7. (a) SiO_2 versus K_2O (after Winchester and Floyd, 1977); (b) Molar $\text{Al}/(\text{K}+\text{Na})$ versus $\text{Al}/(\text{Ca}+\text{Na}+\text{K})$ diagram; (c) $10000*\text{Ga}/\text{Al}$ versus FeOt/MgO , and (d) $\text{Zr}+\text{Nb}+\text{Ce}+\text{Y}$ versus $10000*\text{Ga}/\text{Al}$ (after Whalen et al., 1987) for the Triassic Group 1 and 2 granites in NW Thailand. Symbols in (b-d) are same in (a).

Fig. 8. Chondrite-normalized REE patterns (a) and primitive mantle-normalized element spiderdiagrams (b) for the Triassic Group 1 and 2 granites in NW Thailand. Normalizing values in (a) and (b) are from Taylor and McLennan (1985) and Sun and McDonough (1989), respectively. The data for the Kwangian and Indosinian granites and Precambrian sedimentary rocks in the South China Block are from Wang et al. (2007, 2013); Zeng et al. (2008); Wan et al. (2010) and Zhang et al. (2014).

Fig. 9. $\epsilon_{\text{Nd}}(t)$ versus initial $^{87}\text{Sr}/^{86}\text{Sr}(t)$ for the Triassic Group 1 and 2 granites in NW Thailand. Data sources are from Li and McCulloch (1996); Healy et al. (2004); Wang et al. (2007, 2013, 2015); Shen et al. (2009); Ma et al. (2015); Peng et al. (2013).

Fig. 10. Plots of Rb/Sr versus Rb/Ba (a), $\text{CaO}/\text{Al}_2\text{O}_3$ versus $\text{Al}_2\text{O}_3/\text{TiO}_2$ (b), $\text{CaO} + \text{MgO} + \text{FeOt} + \text{TiO}_2$ versus $\text{Al}_2\text{O}_3 + \text{MgO} + \text{FeOt} + \text{TiO}_2$ (c) and $\text{CaO}/(\text{MgO} + \text{FeOt} + \text{TiO}_2)$ versus $\text{Al}_2\text{O}_3/(\text{MgO} + \text{FeOt} + \text{TiO}_2)$ (d) for the Triassic Group 1 and 2 granites in NW Thailand. Fields are from Dounce and Harris (1998), Sylvester et al. (1998) and Wang et al. (2007, 2013). Symbols in (b-d) are as same in (a).

Fig. 11. Plots of (a) A/CNK and $\epsilon_{\text{Nd}}(t)$, (b) Hf/Sm and Zr/Y and (c) La/Nb and Zr/Nb for the Triassic Group 1 and 2 granites in NW Thailand, respectively. Symbols in (b-d) are as same in (a).

Fig. 12. Age (Ma) versus $\epsilon_{\text{Hf}}(t)$ (a), T_{DM} model age (b) and $\delta^{18}\text{O}$ values (c) with the insets showing their frequency for the Triassic Group 1 and 2 granites in NW Thailand, respectively. Symbols in (b-d) are as same in (a).

Fig. 13. $\epsilon_{\text{Hf}}(t)$ versus $\delta^{18}\text{O}$ for the Triassic granite for the Group 1 and 2 granites in NW Thailand. Data for mantle zircons, typical S-type granite in Lachlan Fold Belt, Triassic Darongshan S-type granites and Hunan granites are from Peck et al. (2004); Valley et al. (2005); Li et al. (2009), Fu et al. (2016); Jiao et al. (2013) and Peng et al. (2016).

Fig. 14 Schematic tectonic cratons showing the Paleotethyan spatial pattern and its tectonic evolution in NW Thailand. See text for the detailed description for (a-d).

Table Captions

Table 1 Summary of sampling locations and zircon U-Pb and in-situ Hf -O analyses of the Triassic granites from the Inthanon and Sukhothai zones in the NW Thailand

Table 2: Zircon in-situ Hf-O isotopic analytical results for the Triassic granites from the Inthanon and Sukhothai zones in NW Thailand

Table 3: Major oxides, trace elemental and Sr-Nd isotopic analytical results for the late Triassic granites from the Inthanon and Sukhothai zones in NW Thailand

Appendix 1

Cathodoluminescence (CL) images of representative zircon grains of these dating samples. Group 1 samples: (a) TG-5A, (b) TG-6A, (c) TG-11A, (d) TG-16B₁, (e) TG-16A₂, (f) TL-26A, (g) TG-42A, (h) TG-53A; Gruop 2 samples: (i) TL-13A₁ and (j) TG-27A

Supplementary Dataset

LA-ICPMS zircon U-Pb dating results of late Triassic granites from the Inthanon and Sukhothai zones in NW Thailand

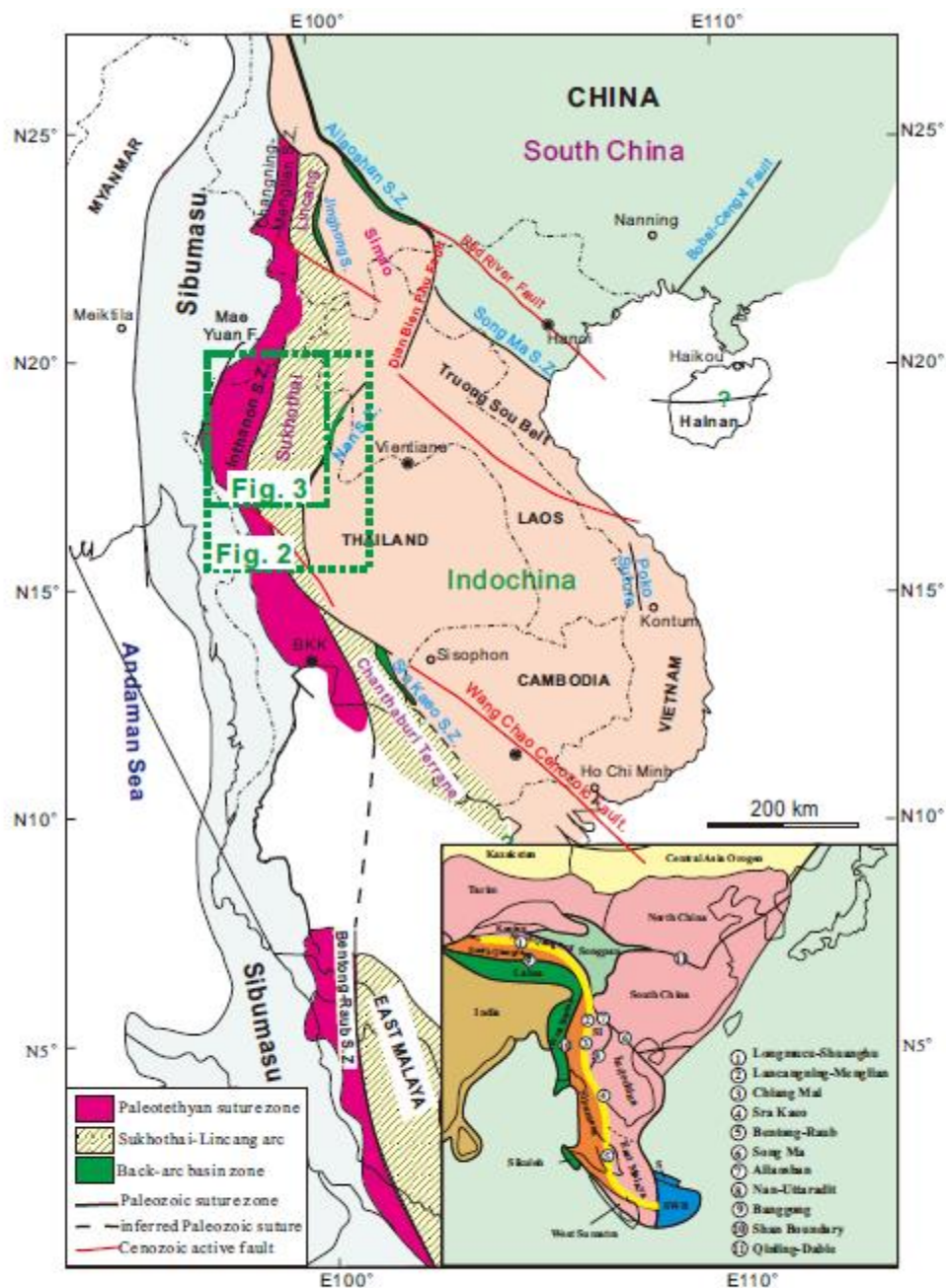


Fig. 1 Y-J Wang & coauthors

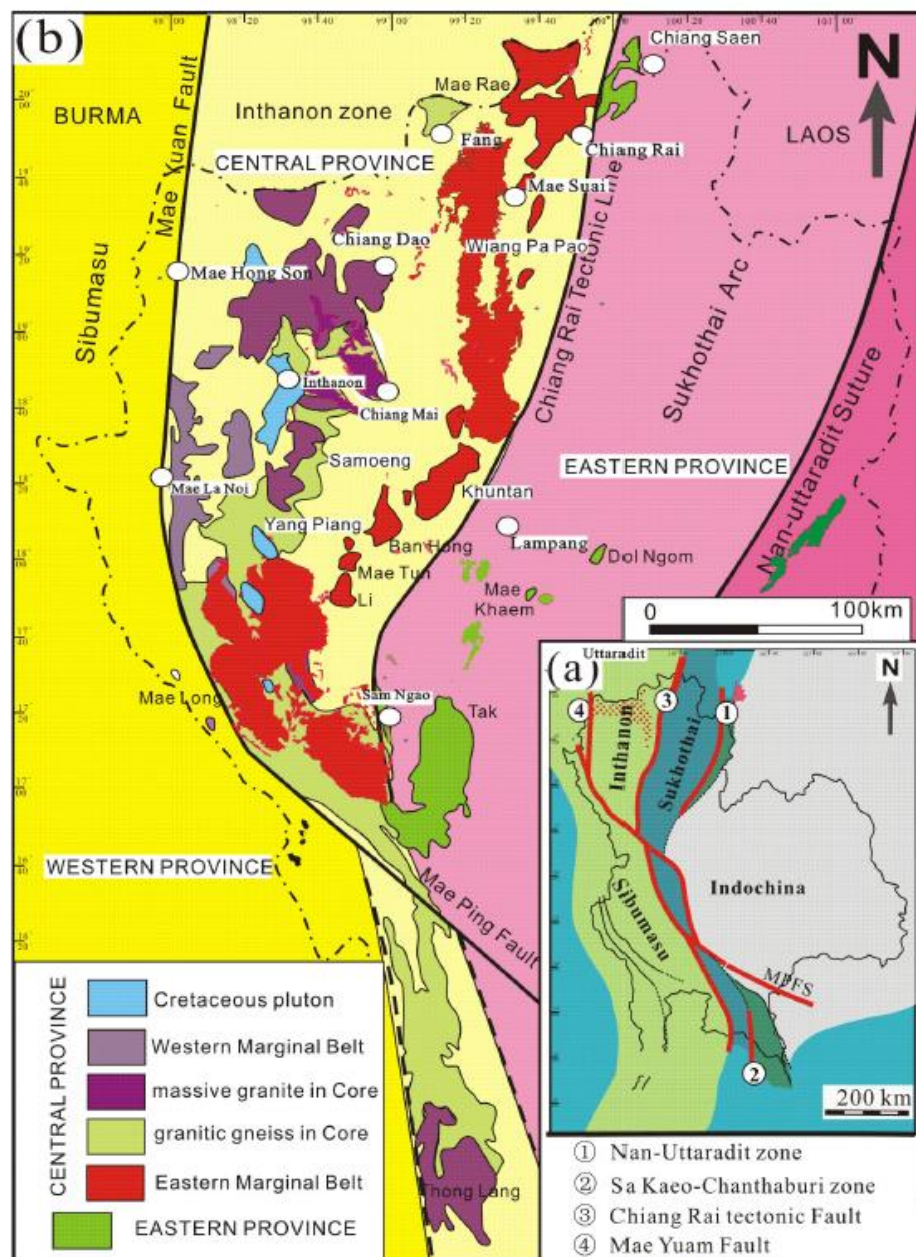


Fig. 2 Y-J Wang & coauthors

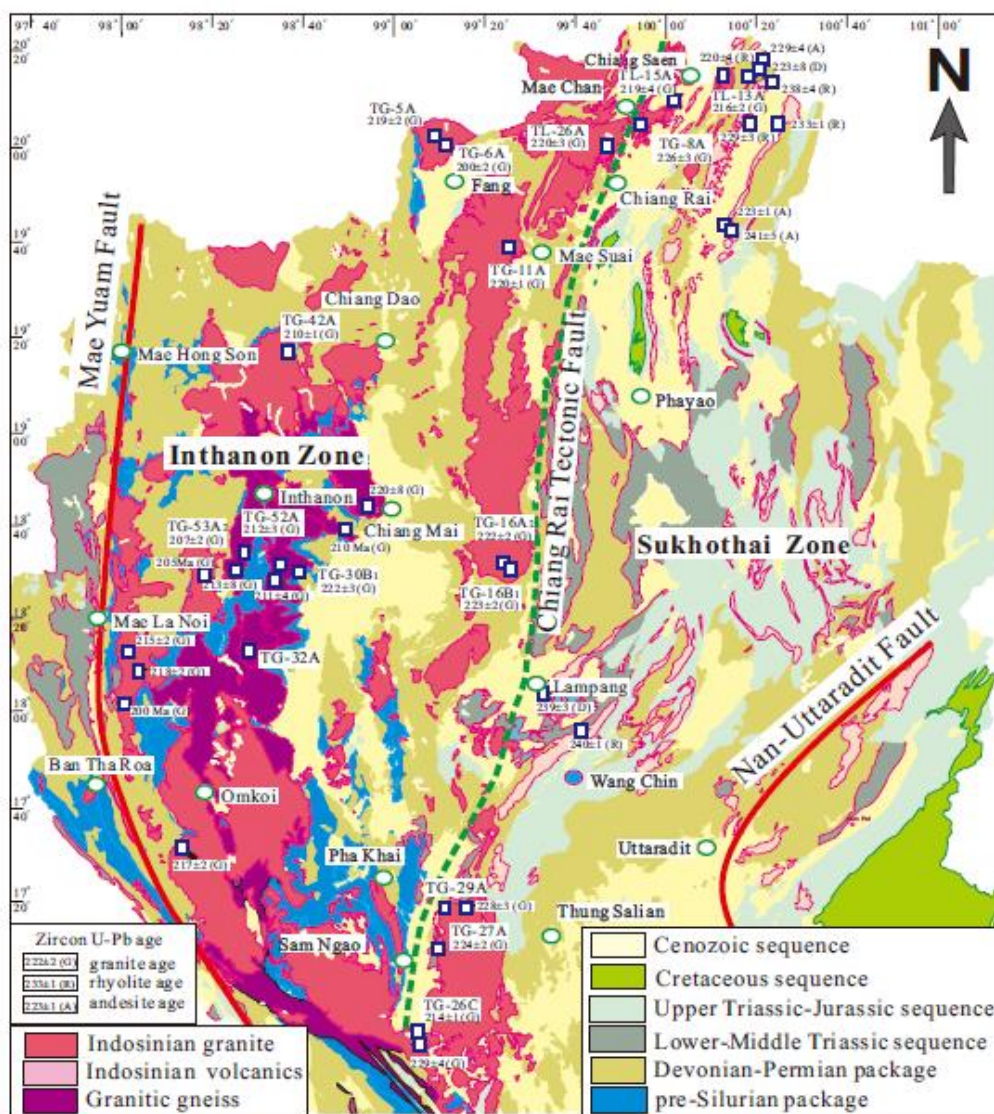


Figure 3 Y-J Wang & coauthors

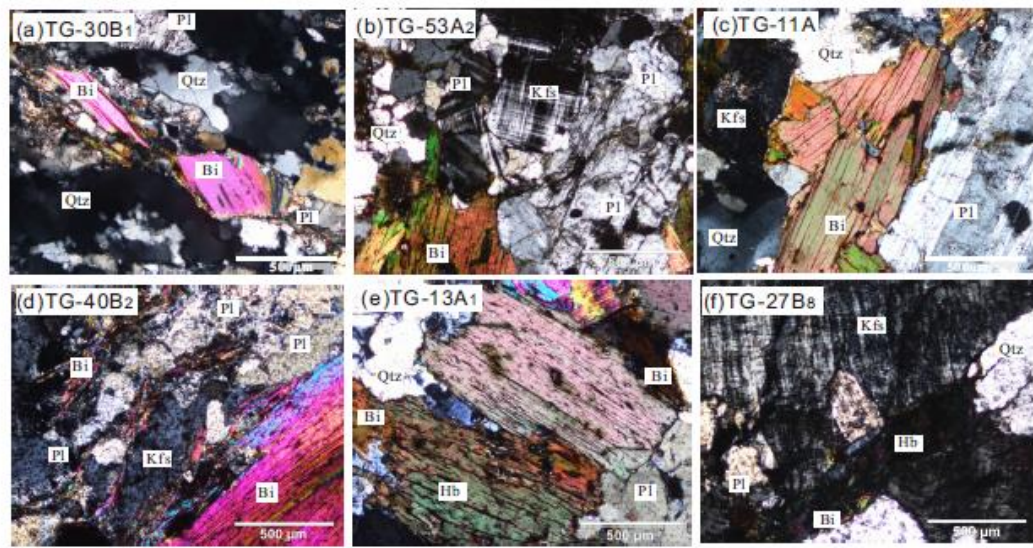


Figure 4 Y-J Wang & coauthors

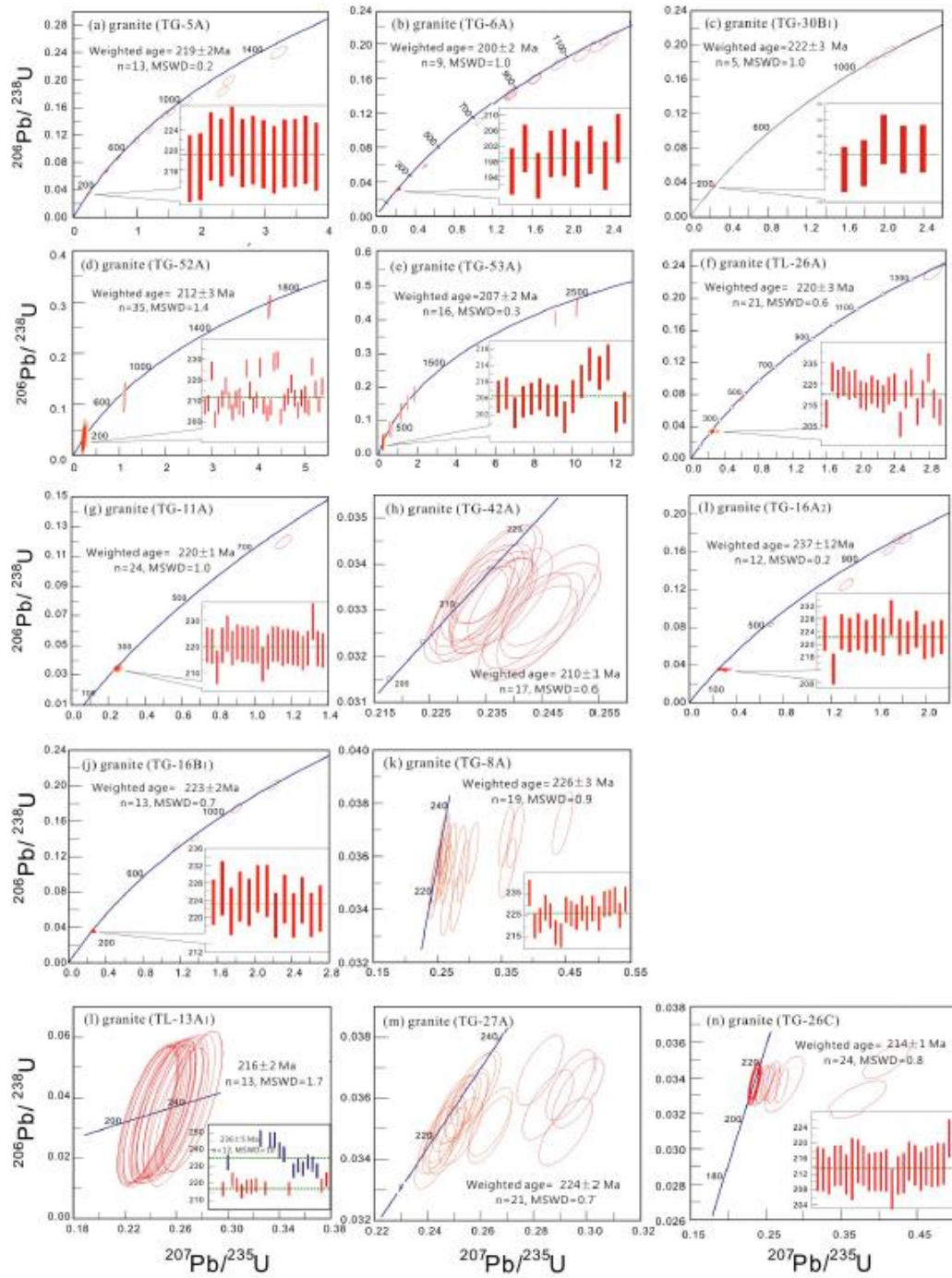


Figure 5 Y-J Wang & coauthors

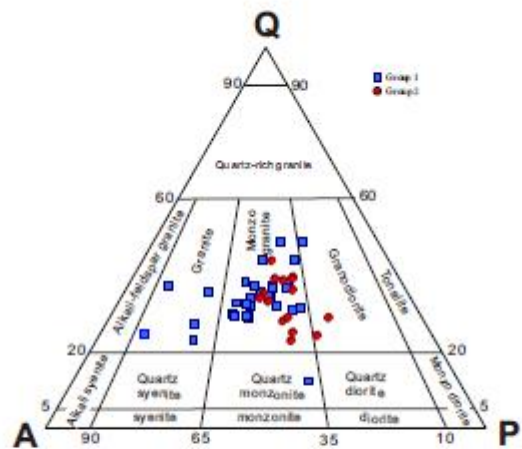


Figure 6 Y-J Wang & coauthors

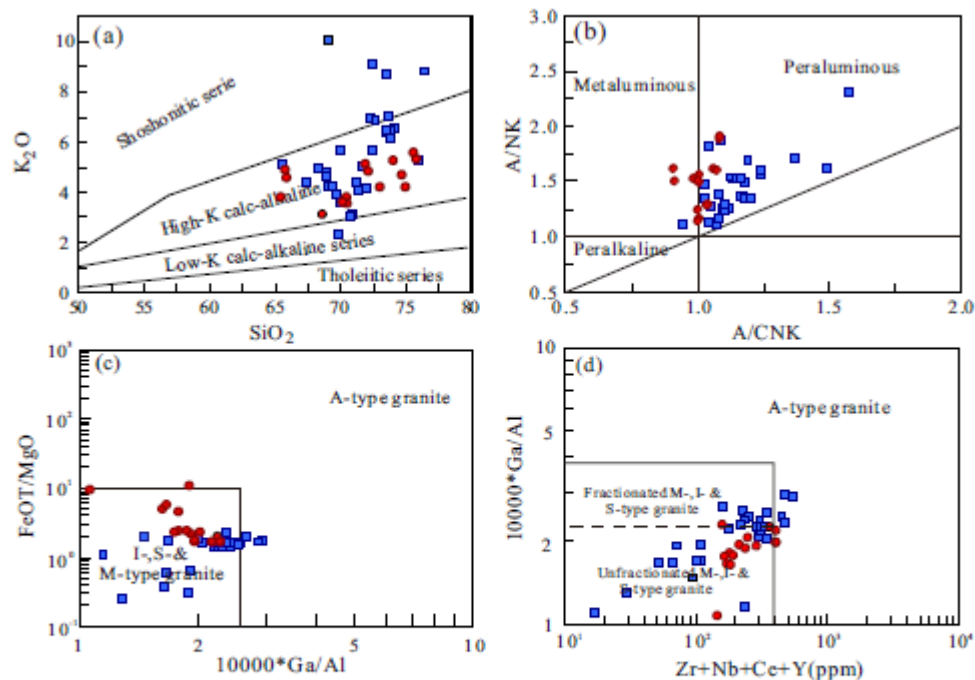


Figure 7 Y-J Wang & coauthors

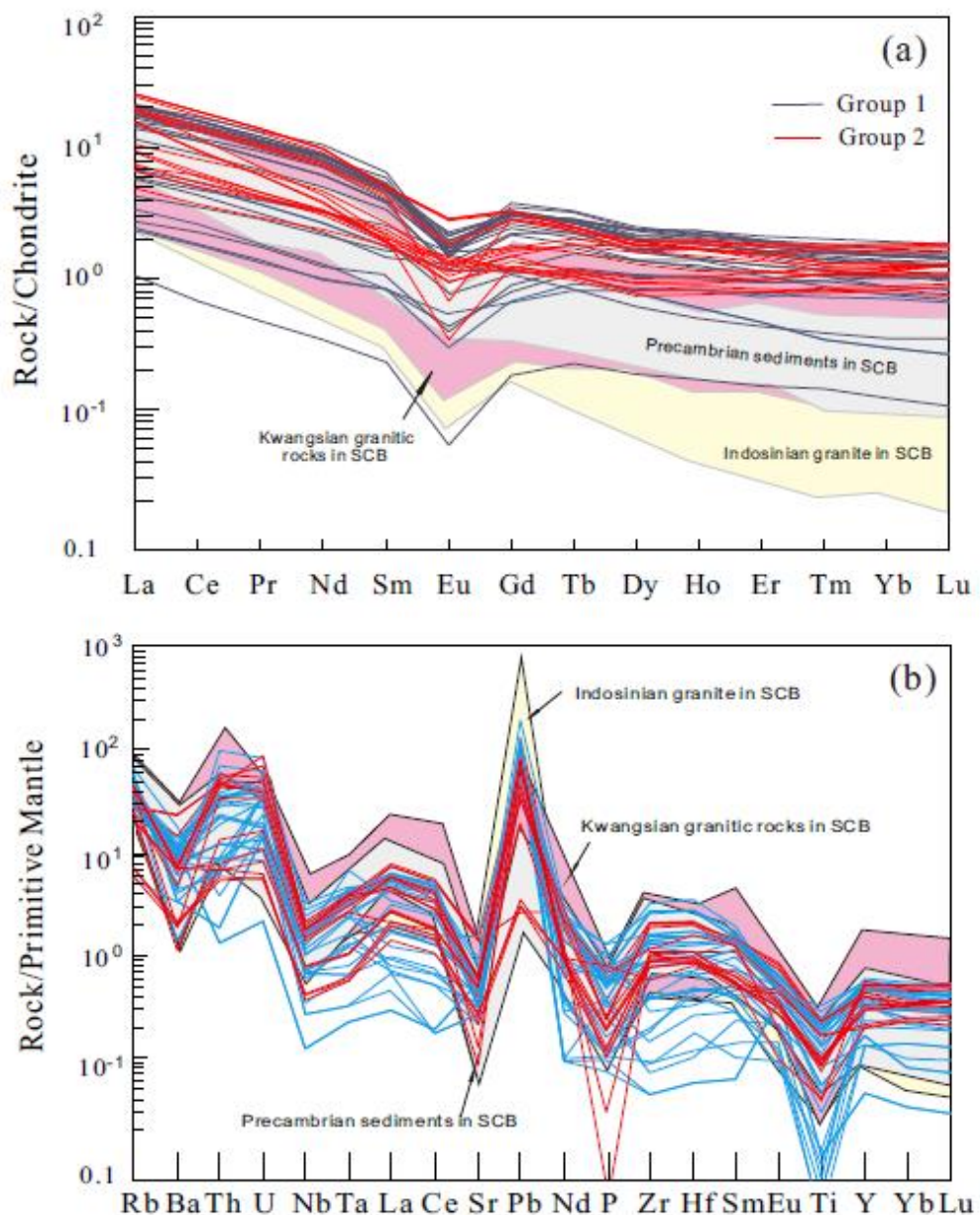


Figure 8 Y-J Wang & coauthors

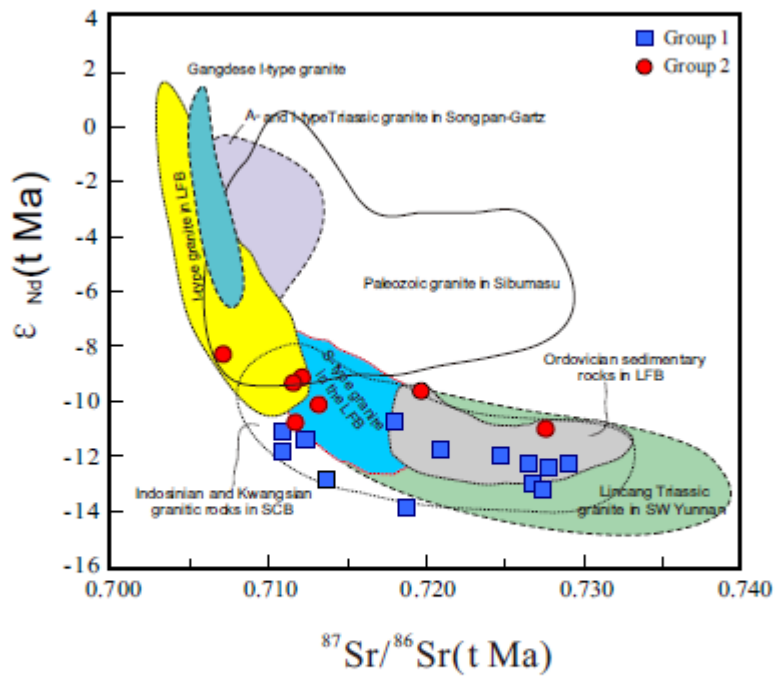


Figure 9 Y-J Wang & coauthors

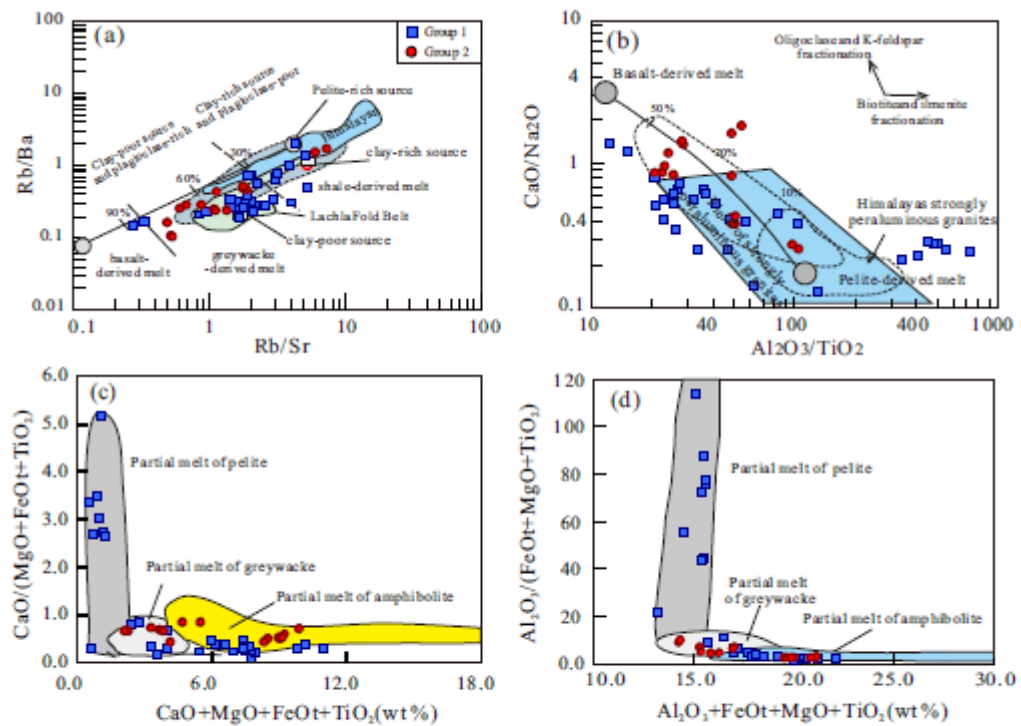


Figure 10 Y-J Wang & coauthors

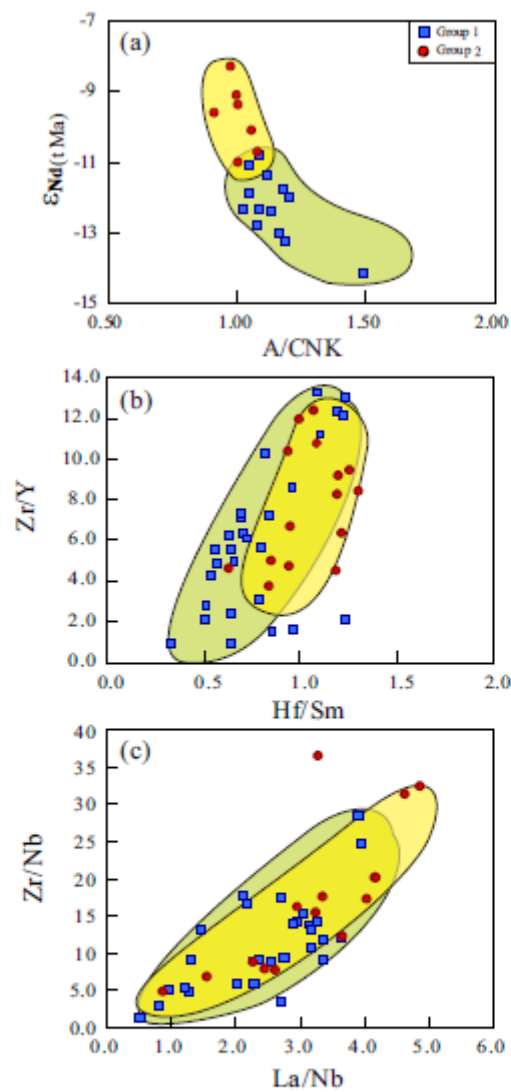


Figure 11 Y-J Wang & coauthors

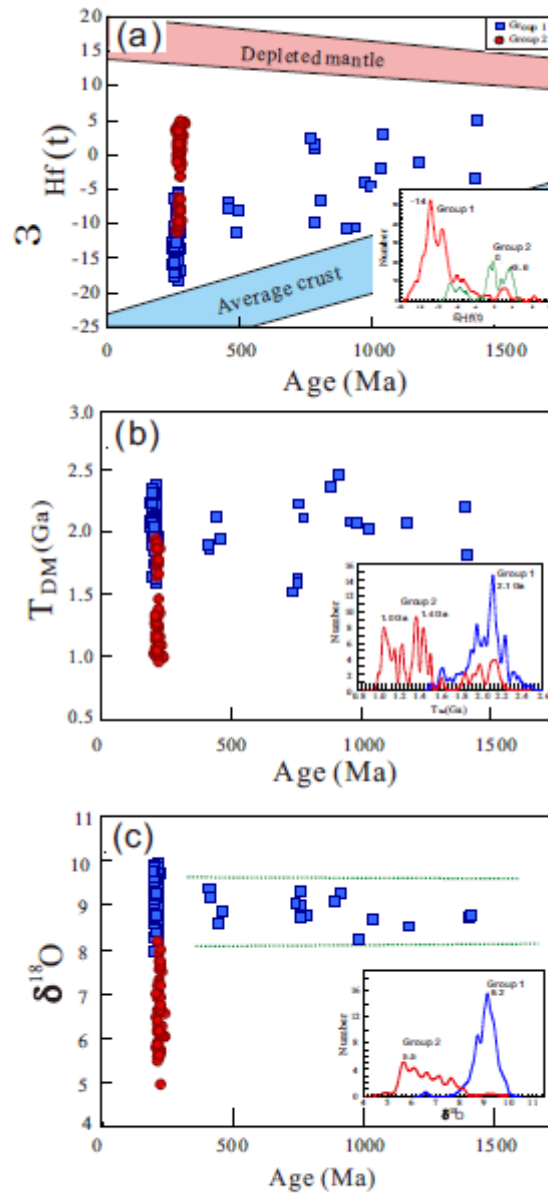


Figure 12 Y-J Wang & coauthors

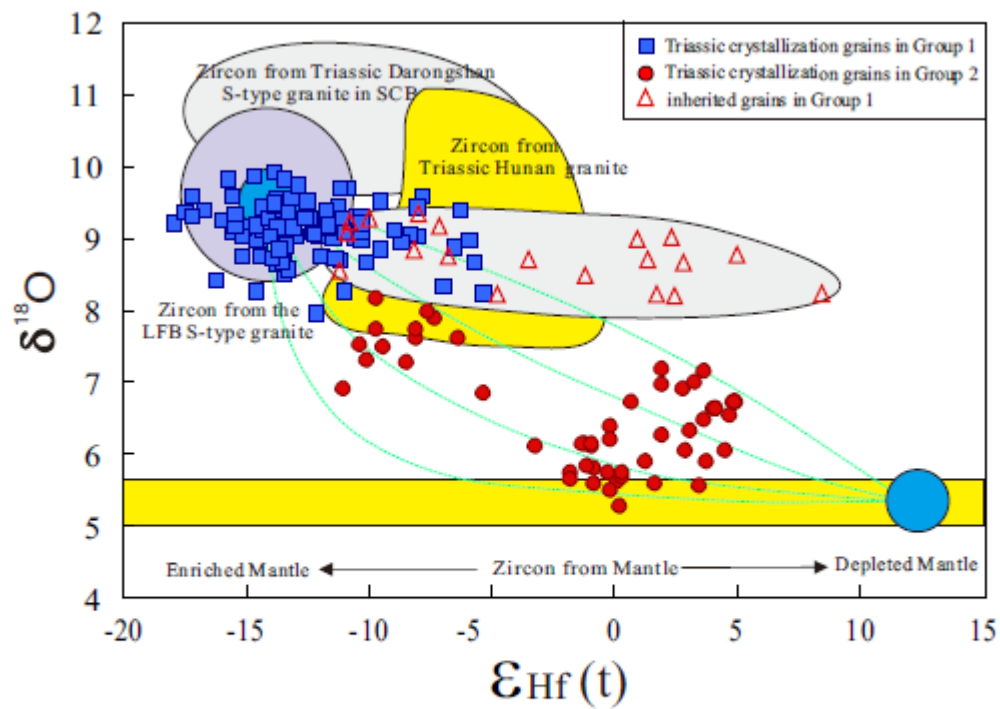


Figure 13 Y-J Wang & coauthors

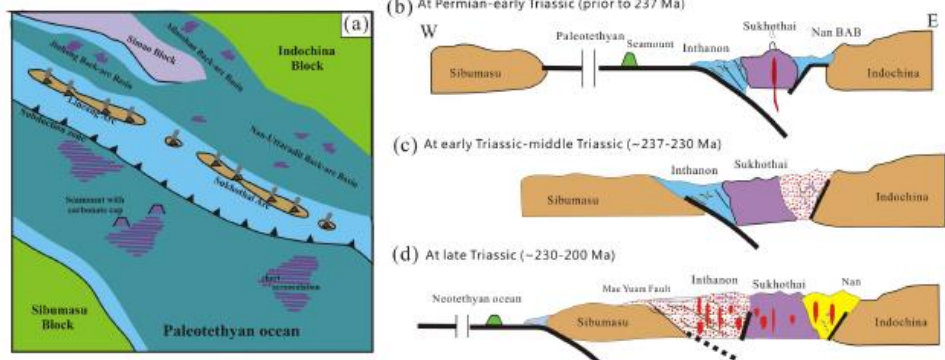
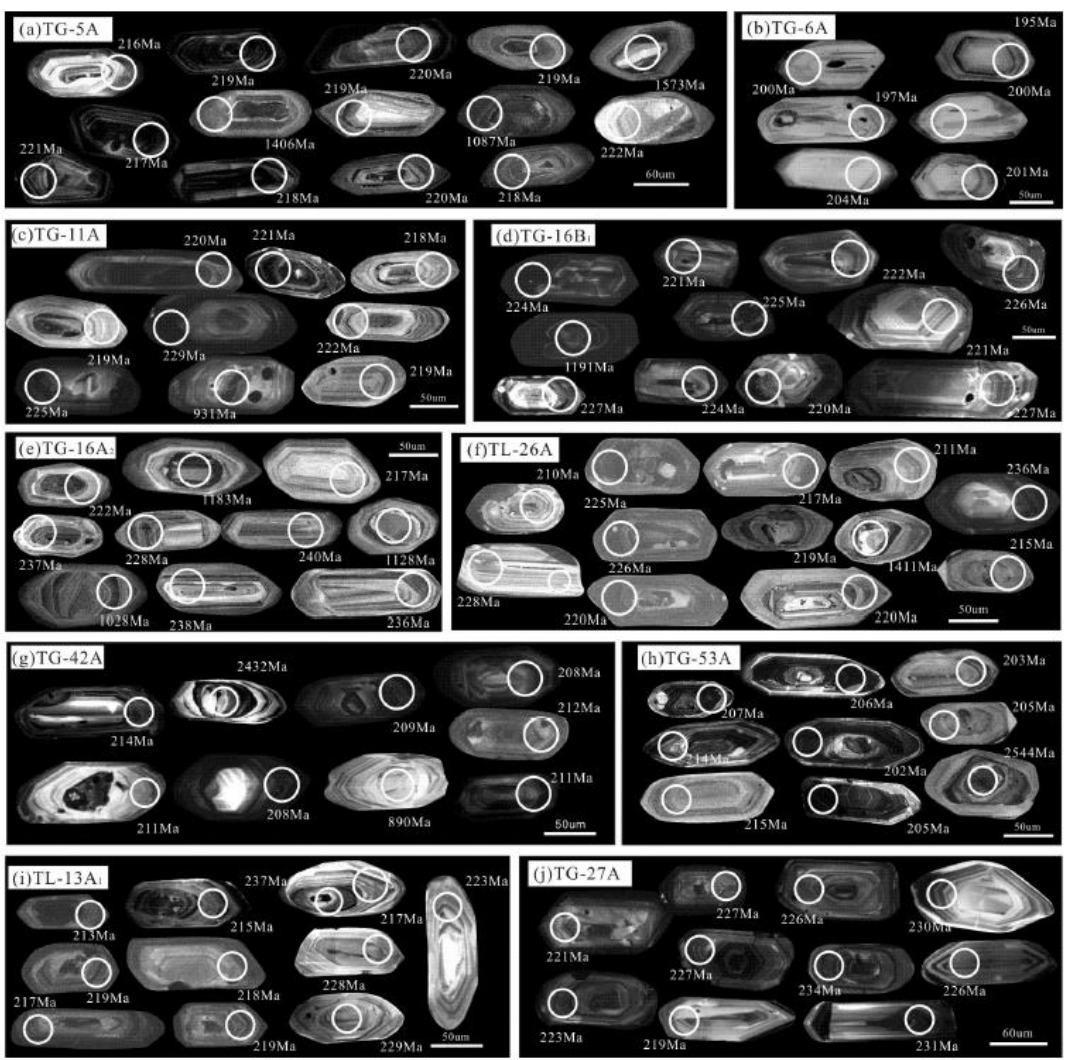


Fig. 14 Y-J Wang & coauthors



Appendix 1

Table 1 Summary of sampling locations and zircon U-Pb and in-situ Hf -O analyses of the Triassic granites from the Inthanon and Sukhothai zones in the NW Thailand

sample	lithology	sampling location	zircon U-Pb crystallization age	Inherited zircon U-Pb age (Ma)	grains for late Triassic crystallization age		
				$\epsilon_{\text{Hf}}(t)$	T _{D_{M2}} (Ga)	$\delta^{18}\text{O}$	
Group 1 samples: Triassic granites in the Inthanon zone to east of the Chiang Rai Fault in NW Thailand							
TG-5A	granitic gneiss	Fang Hotspring National Park; N 19°57'58", E 99°09'12"	219 ± 2 Ma, n=13, MSWD=0.2	419, 422, 541, 682, 775, 899, 1010, 1087, 1406, 1489, 1573	-10.9~15.1	1.92-2.21	8.69-9.41 (8.95±0.17)
TG-6A	granitic gneiss	Southeast of Fang Hotspring National Park; N 19°57'12", E 99°09'39"	200 ± 2 Ma, n= 9, MSWD=1.0	364, 616, 674, 838, 857, 859, 1051, 1056, 1120, 1276, 1283, 2457			
TG-30B ₁	granitic gneiss	Inthanon National Park; N18°29'41", E 98°40'04"	222 ± 3 Ma, n=5, MSWD=1.0	1080, 1131			
TG-52A	mylonitic granite	Doi Inthanon	212 ± 3 Ma, n=35, MSWD=1.4	254, 691, 695, 1729, 1731	-9.6~21.0	1.86-2.33	8.82-9.86 (9.24±0.12)
TG-53A	mylonitic granite	Doi Inthanon	207 ± 2 Ma, n=16, MSWD=0.3	450, 461, 743, 762, 922, 1097, 2490, 2544	-10.3~15.7	1.90-2.24	8.56-9.84 (9.18± 0.24)
TL-26A	porphyritic granite	Sleeping Buddha Park of Wat Ban San Phatthana; N 20°07'30", E 99°51'11"	220 ± 3 Ma, n=21, MSWD=0.6	260, 466, 1411	-5.4~12.1	1.60~2.02	7.95-9.71 (8.93± 0.23)
TG-11A	porphyritic granite	Mae Wiang Pa Pao; N 19°41'36", E99°25'06"	220 ± 1 Ma, n=24, MSWD=1.0	727			
TG-42A	porphyritic granite	At 85 km Marker of 1095 Highway, N19°17'04", E98°29'09"	210 ± 1 Ma, n=17, MSWD=0.6	890, 2432	-10.3~17.7	1.90-2.36	8.28-9.59 (9.24±0.16)
TG-16A ₂	granitic gneiss enclave	Khun Tan granitic pluton; N 18°27'22", E99°11'35"	237 ± 12 Ma, n=12, MSWD=0.2	507, 1028, 1083, 1129	-10.9~15.6	1.95-2.24	8.73-9.94 (9.30±0.25)
TG-16B ₁	porphyritic granite	Khun Tan granitic pluton; N 18°27'22", E99°11'35"	223 ± 2 Ma, n=13, MSWD=0.7	787, 851, 1133, 1191	-11.5~16.7	1.99-2.31	6.59-9.56 (9.12±0.24)
Group 2 samples: Triassic granites in the Sukhothai zone to east of the Chiang Rai Fault in NW Thailand							
TG-8A	porphyritic granite	Mae Chan granitic pluton, N 20°07'35", E99°52'00"	226 ± 3 Ma, n=19, MSWD=0.9		-6.2~11.1	1.65-1.95	6.89-9.26 (7.66±0.19)
TL-13A ₁	monzonitic granite	Wat Kio Kan; N 20°19'32", E100°18'33"		236 ± 5 Ma, n=12, MSWD=1.0	+0.7~+4.8	0.96~1.23	6.02-7.16 (6.65± 0.28) 5.88~7.17 (6.63± 0.37)
TG-26C	granite	Lang Sang Park at 12 km to Tak, N 16°46'59", E 99°01'04"	214 ± 1 Ma, n=24, MSWD=0.8		+1.2~+4.1	1.00~1.18	

TG-27A	monzonitic granite	20 km northeast toward Tak; N17°07'55", E99°06'11"	224 ± 2 Ma, n=21, MSWD=0.7	-3.2~+3.4	1.04-1.47	4.95-6.38 (5.78±0.14)
--------	--------------------	--	----------------------------	-----------	-----------	--------------------------

note: $^{206}\text{Pb}/^{238}\text{U}$ apparent age is used when zircon analytical spots with the age of younger than 1000 Ma and $^{207}\text{Pb}/^{206}\text{Pb}$ apparent age is listed for zircon with the age of older than 1000 Ma.

Table 2: Zircon in-situ Hf-O isotopic analytical results for the Triassic granites from the Inthanon and Sukhothai zones in NW Thailand

analytical spot	Apparent age (Ma)	$^{176}\text{Hf}/^{177}\text{Hf}$	2σ	$^{176}\text{Lu}/^{177}\text{Hf}$	$^{176}\text{Yb}/^{177}\text{Hf}$	$\epsilon\text{Hf(t)}$	2σ	T_{DM}	2σ	$\delta^{18}\text{O}$	2σ
Group 1 samples: Triassic granites in the Inthanon zones to west of the Chiang Rai Fault in NW Thailand											
TG-5A, granitic gneiss, Hot spring National Park in Fang; N 19°57'58", E 99°09'12"											
TG-5A-01	216	0.282267	0.000013	0.000807	0.019683	-13.2	0.5	2.09	0.03	9.41	0.37
TG-5A-02	920	0.281915	0.000018	0.000990	0.025017	-10.6	0.6	2.47	0.04	9.24	0.29
TG-5A-03	217	0.282235	0.000014	0.001028	0.024953	-14.4	0.5	2.16	0.03	8.96	0.34
TG-5A-06	892	0.281993	0.000013	0.000550	0.014309	-10.8	0.4	2.37	0.03	9.09	0.25
TG-5A-07	917	0.282287	0.000015	0.000440	0.010394	2.5	0.5	1.63	0.03	8.21	0.25
TG-5A-08	221	0.282257	0.000016	0.001630	0.040912	-13.6	0.6	2.12	0.04	9.06	0.27
TG-5A-09	422	0.282328	0.000012	0.002265	0.056591	-7.0	0.4	1.86	0.03	9.18	0.23
TG-5A-10	419	0.282303	0.000013	0.001745	0.042790	-7.9	0.5	1.91	0.03	9.35	0.25
TG-5A-11	219	0.282323	0.000010	0.000621	0.015312	-11.2	0.4	1.96	0.02	8.69	0.19
TG-5A-12	222	0.282123	0.000011	0.000658	0.015019	-18.2	0.4	2.40	0.02	9.21	0.36
TG-5A-13	219	0.282332	0.000016	0.001129	0.027407	-10.9	0.6	1.95	0.04	9.10	0.36
TG-5A-14	220	0.282294	0.000015	0.001245	0.030521	-12.3	0.5	2.03	0.03	9.11	0.37
TG-5A-15	219	0.282229	0.000015	0.000901	0.022413	-14.5	0.5	2.17	0.03	8.99	0.28
TG-5A-16	218	0.282342	0.000015	0.001087	0.026967	-10.6	0.5	1.92	0.03	9.02	0.20
TG-5A-17	1406	0.281954	0.000016	0.000532	0.012667	-3.4	0.6	2.22	0.04	8.72	0.40
TG-5A-18	219	0.282275	0.000011	0.001524	0.037860	-13.0	0.4	2.08	0.02	9.04	0.36
TG-5A-19	769	0.282074	0.000014	0.000410	0.009514	-9.9	0.5	2.24	0.03	9.29	0.33
TG-5A-20	219	0.282213	0.000013	0.001197	0.029557	-15.1	0.5	2.21	0.03	8.74	0.32
TG-16A ₂ , granitic gneiss enclave in the Khun Tan pluton; N 18°27'22", E 99°11'35"											
TG-16A ₂ -02	223	0.282235	0.000015	0.000401	0.009404	-14.1	0.5	2.15	0.03	9.19	0.16
TG-16A ₂ -03	1031	0.282090	0.000013	0.001372	0.031985	-2.2	0.5	2.03	0.03		
TG-16A ₂ -04	212	0.282259	0.000014	0.000481	0.011429	-13.6	0.5	2.11	0.03	9.26	0.18
TG-16A ₂ -05	224	0.282283	0.000012	0.000559	0.013541	-12.5	0.4	2.05	0.03	9.50	0.18
TG-16A ₂ -06	223	0.282305	0.000015	0.000735	0.018494	-11.7	0.5	2.00	0.03	9.24	0.14
TG-16A ₂ -09	224	0.282327	0.000016	0.001167	0.029122	-11.0	0.6	1.96	0.04	9.16	0.13
TG-16A ₂ -10	762	0.282343	0.000015	0.001346	0.030608	1.0	0.5	1.62	0.03	8.99	0.10
TG-16A ₂ -11	222	0.282232	0.000016	0.000568	0.013804	-14.3	0.6	2.16	0.04	9.12	0.10
TG-16A ₂ -12	223	0.282300	0.000019	0.001689	0.040770	-12.1	0.7	2.02	0.04	9.03	0.14
TG-16A ₂ -13	222	0.282247	0.000012	0.001163	0.028186	-13.9	0.4	2.13	0.03	9.94	0.12

TG-16A ₂ -14	228	0.282327	0.000015	0.001059	0.025890	-10.9	0.5	1.95	0.03	9.72	0.13
TG-16A ₂ -15	222	0.282196	0.000013	0.000926	0.021980	-15.6	0.4	2.24	0.03		
TG-16A ₂ -16	222	0.282260	0.000017	0.001299	0.033392	-13.4	0.6	2.11	0.04	9.84	0.14
TG-16A ₂ -17	225	0.282196	0.000014	0.000599	0.014508	-15.5	0.5	2.24	0.03	9.09	0.13
TG-16A ₂ -19	965	0.282085	0.000014	0.001605	0.039834	-4.0	0.5	2.09	0.03		
TG-16A ₂ -20	221	0.282259	0.000013	0.000790	0.019073	-13.4	0.5	2.10	0.03	8.73	0.11

TG-16B₁, porphyritic granite from the Khun Tan granitic pluton; N 18°27'22", E 99°11'35"

TG-16B ₁ -01	1178	0.282018	0.000013	0.000742	0.018176	-1.2	0.5	2.08	0.03	8.50	0.13
TG-16B ₁ -02	224	0.282255	0.000019	0.000557	0.013706	-13.5	0.7	2.11	0.04	8.52	0.21
TG-16B ₁ -06	787	0.282094	0.000013	0.000126	0.003386	-6.7	0.5	2.12	0.03	8.76	0.13
TG-16B ₁ -07	227	0.282164	0.000013	0.000881	0.021984	-16.7	0.5	2.31	0.03		
TG-16B ₁ -09	221	0.282213	0.000015	0.000827	0.020852	-15.0	0.5	2.21	0.03	9.15	0.14
TG-16B ₁ -10	225	0.282311	0.000014	0.000630	0.015527	-11.5	0.5	1.99	0.03	9.00	0.10
TG-16B ₁ -12	224	0.282313	0.000016	0.001926	0.047927	-11.6	0.6	2.00	0.04	9.15	0.12
TG-16B ₁ -13	227	0.282249	0.000015	0.000863	0.020519	-13.7	0.5	2.12	0.03	9.41	0.12
TG-16B ₁ -14	1036	0.282215	0.000018	0.000560	0.012771	2.8	0.6	1.71	0.04	8.68	0.14
TG-16B ₁ -15	226	0.282269	0.000016	0.001440	0.036915	-13.1	0.6	2.09	0.03	9.16	0.13
TG-16B ₁ -17	221	0.282251	0.000013	0.000661	0.015916	-13.7	0.5	2.12	0.03	8.67	0.15
TG-16B ₁ -19	224	0.282280	0.000016	0.000923	0.022870	-12.6	0.5	2.06	0.03	8.59	0.17
TG-16B ₁ -20	220	0.282252	0.000015	0.000945	0.023741	-13.7	0.5	2.12	0.03	9.56	0.15

TL-26A, porphyritic granite, Sleeping Buddha Park of Wat Ban San Phatthana; N 20°07'30", E 99°51'11"

TL-26A-1	210	0.282304	0.000016	0.001381	0.034539	-12.1	0.6	2.02	0.04	7.95	0.26
TL-26A-2	228	0.282318	0.000015	0.000569	0.014191	-11.1	0.5	1.97	0.03	9.71	0.34
TL-26A-3	225	0.282408	0.000020	0.000577	0.014499	-8.0	0.7	1.77	0.04	9.03	0.28
TL-26A-4	226	0.282400	0.000014	0.000873	0.021283	-8.3	0.5	1.79	0.03	9.05	0.27
TL-26A-5	224	0.282389	0.000017	0.000606	0.014921	-8.7	0.6	1.81	0.04	8.95	0.35
TL-26A-6	225	0.282365	0.000015	0.000473	0.010262	-9.5	0.5	1.86	0.03	8.84	0.21
TL-26A-7	220	0.282387	0.000014	0.000807	0.019233	-8.9	0.5	1.82	0.03	9.14	0.24
TL-26A-8	219	0.282349	0.000018	0.000739	0.018061	-10.3	0.6	1.91	0.04	8.98	0.27
TL-26A-9	1411	0.282083	0.000017	0.000627	0.014948	5.0	0.6	1.82	0.04	8.78	0.16
TL-26A-10	222	0.282485	0.000018	0.000695	0.014028	-5.4	0.6	1.60	0.04	8.22	0.31
TL-26A-11	220	0.282354	0.000016	0.001216	0.030551	-10.1	0.6	1.90	0.04	8.66	0.31
TL-26A-12	217	0.282329	0.000017	0.000633	0.015053	-11.0	0.6	1.95	0.04	8.28	0.33
TL-26A-13	221	0.282474	0.000016	0.000399	0.009801	-5.7	0.6	1.62	0.04	8.65	0.34

TL-26A-14	223	0.282440	0.000015	0.000648	0.015517	-6.9	0.5	1.70	0.03	8.33	0.34
TL-26A-15	205	0.282470	0.000017	0.000772	0.017195	-6.3	0.6	1.64	0.04	9.40	0.22
TL-26A-16	220	0.282472	0.000015	0.000501	0.012154	-5.9	0.5	1.63	0.03	8.98	0.22
TL-26A-17	225	0.282452	0.000015	0.000968	0.022298	-6.5	0.5	1.68	0.03	8.88	0.37
TL-26A-18	211	0.282421	0.000014	0.000544	0.012798	-7.9	0.5	1.75	0.03	9.58	0.31
TL-26A-19	220	0.282412	0.000014	0.000880	0.020750	-8.0	0.5	1.77	0.03	9.45	0.23
TL-26A-20	466	0.282258	0.000017	0.000366	0.009617	-8.0	0.6	1.96	0.04	8.85	0.26
TG-42A, porphyritic granite, 85 km Marker of 1095 Highway; N 19°17'04", E 98°29'08"											
TG-42A-01	214	0.282347	0.000021	0.001098	0.026613	-10.5	0.7	1.92	0.05	9.33	0.25
TG-42A-03	209	0.282174	0.000010	0.000909	0.022320	-16.7	0.3	2.30	0.02	9.41	0.17
TG-42A-04	211	0.282258	0.000014	0.001533	0.037463	-13.8	0.5	2.12	0.03	8.62	0.35
TG-42A-05	210	0.282237	0.000014	0.001684	0.041530	-14.6	0.5	2.17	0.03	9.20	0.25
TG-42A-21	208	0.282294	0.000012	0.001011	0.021859	-12.5	0.4	2.04	0.03	9.52	0.19
TG-42A-07	210	0.282233	0.000013	0.001208	0.030017	-14.6	0.5	2.17	0.03	8.28	0.39
TG-42A-08	206	0.282330	0.000012	0.001028	0.025324	-11.2	0.4	1.96	0.03	9.42	0.24
TG-42A-09	211	0.282333	0.000014	0.001001	0.025157	-11.1	0.5	1.95	0.03	9.29	0.26
TG-42A-10	209	0.282145	0.000013	0.001044	0.026524	-17.7	0.4	2.36	0.03	9.38	0.23
TG-42A-11	210	0.282243	0.000015	0.001225	0.030890	-14.3	0.5	2.15	0.03	9.43	0.27
TG-42A-22	212	0.282219	0.000014	0.001538	0.037334	-15.1	0.5	2.20	0.03	9.04	0.27
TG-42A-23	211	0.282241	0.000016	0.001367	0.034249	-14.3	0.5	2.15	0.03	8.75	0.29
TG-42A-25	214	0.282186	0.000017	0.000883	0.020808	-16.2	0.6	2.27	0.04	8.41	0.31
TG-42A-15	208	0.282300	0.000012	0.000831	0.020633	-12.2	0.4	2.02	0.03	9.06	0.28
TG-42A-16	209	0.282247	0.000014	0.000981	0.024308	-14.1	0.5	2.14	0.03	9.29	0.28
TG-42A-17	987	0.282115	0.000013	0.001824	0.045508	-4.7	0.4	2.08	0.03	8.22	0.27
TG-42A-18	211	0.282159	0.000013	0.000915	0.022424	-17.2	0.5	2.33	0.03	9.59	0.27
TG-42A-19	212	0.282355	0.000015	0.001306	0.032031	-10.3	0.5	1.90	0.03	9.32	0.18
TG-52A, granitic gneiss, Doi Inthanon											
TG-52A-01	208	0.282167	0.000011	0.002522	0.060452	-17.2	0.4	2.33	0.02	9.31	0.30
TG-52A-02	209	0.282265	0.000012	0.003055	0.074763	-13.8	0.4	2.12	0.03	9.16	0.32
TG-52A-03	224	0.282264	0.000012	0.002061	0.050572	-13.3	0.4	2.10	0.03	8.92	0.19
TG-52A-04	201	0.282205	0.000013	0.002378	0.057460	-15.9	0.5	2.25	0.03	9.26	0.32
TG-52A-05	208	0.282259	0.000010	0.001267	0.031303	-13.8	0.4	2.12	0.02	9.47	0.26
TG-52A-07	217	0.282311	0.000012	0.000978	0.024048	-11.7	0.4	1.99	0.03	9.41	0.20
TG-52A-08	210	0.282255	0.000014	0.001381	0.034825	-13.9	0.5	2.12	0.03	9.48	0.38

TG-52A-09	204	0.282360	0.000014	0.001400	0.034602	-10.3	0.5	1.89	0.03	9.10	0.23
TG-52A-11	211	0.282215	0.000014	0.002681	0.064822	-15.4	0.5	2.22	0.03	9.19	0.33
TG-52A-12	1729	0.282024	0.000012	0.001201	0.030151	8.4	0.4	1.77	0.03	8.06	0.19
TG-52A-13	210	0.282322	0.000014	0.002378	0.058591	-11.6	0.5	1.98	0.03	9.18	0.35
TG-52A-14	206	0.282238	0.000015	0.002116	0.051719	-14.7	0.5	2.17	0.03	9.86	0.32
TG-52A-15	226	0.282207	0.000013	0.003330	0.081886	-15.5	0.5	2.24	0.03	9.58	0.28
TG-52A-16	215	0.282273	0.000017	0.001810	0.047065	-13.2	0.6	2.09	0.04	9.57	0.29
TG-52A-17	208	0.282252	0.000013	0.001296	0.032782	-14.0	0.5	2.13	0.03	9.03	0.19
TG-52A-18	211	0.282375	0.000014	0.001100	0.027362	-9.6	0.5	1.86	0.03	9.52	0.25
TG-52A-19	226	0.282203	0.000012	0.001607	0.040141	-15.4	0.4	2.23	0.03	9.36	0.30
TG-52A-20	208	0.282341	0.000015	0.002196	0.054126	-11.0	0.5	1.94	0.03	9.11	0.25

TG-53A, granitic gneiss, Doi Inthanon

TG-53A-01	450	0.282194	0.000017	0.001599	0.038665	-11.0	0.6	2.14	0.04	8.57	0.32
TG-53A-02	206	0.282357	0.000016	0.000946	0.023480	-10.3	0.5	1.90	0.03	9.22	0.20
TG-53A-03	207	0.282276	0.000013	0.001351	0.032630	-13.2	0.5	2.08	0.03	8.56	0.28
TG-53A-04	203	0.282268	0.000014	0.001281	0.031798	-13.5	0.5	2.10	0.03	8.67	0.28
TG-53A-05	922	0.282297	0.000016	0.002972	0.072441	1.7	0.6	1.69	0.04	8.23	0.27
TG-53A-06	205	0.282255	0.000011	0.000663	0.015960	-13.9	0.4	2.12	0.02	8.72	0.36
TG-53A-07	206	0.282206	0.000013	0.001514	0.037212	-15.7	0.4	2.24	0.03	9.84	0.24
TG-53A-08	207	0.282311	0.000014	0.001087	0.028014	-11.9	0.5	2.00	0.03	8.76	0.25
TG-53A-12	205	0.282265	0.000014	0.001148	0.028995	-13.6	0.5	2.10	0.03	8.84	0.32
TG-53A-13	201	0.282288	0.000016	0.001001	0.024776	-12.8	0.5	2.05	0.03	9.74	0.18
TG-53A-14	762	0.282351	0.000013	0.001060	0.026314	1.4	0.5	1.59	0.03	8.71	0.23
TG-53A-16	207	0.282273	0.000015	0.000867	0.019456	-13.3	0.5	2.08	0.03	9.37	0.22
TG-53A-17	210	0.282297	0.000013	0.001044	0.025851	-12.3	0.5	2.03	0.03	9.30	0.14
TG-53A-18	214	0.282286	0.000015	0.001045	0.025422	-12.6	0.5	2.05	0.03	9.27	0.22
TG-53A-19	743	0.282389	0.000012	0.001062	0.026359	2.3	0.4	1.52	0.03	9.01	0.27
TG-53A-20	212	0.282327	0.000011	0.001779	0.043050	-11.3	0.4	1.97	0.02	8.74	0.22

Group 2 samples: Triassic granites in the Sukhothai zones to east of the Chiang Rai Fault in NW Thailand

TG-8A, porphyritic granite, Mae Chan pluton, N 20°07'35", E 99°52'00"											
TG-8A-01	236	0.282368	0.000017	0.002309	0.057057	-9.5	0.6	1.87	0.04	7.48	0.27
TG-8A-03	220	0.282364	0.000021	0.000977	0.023840	-9.7	0.7	1.87	0.05	7.16	0.17
TG-8A-04	223	0.282430	0.000015	0.000889	0.019528	-7.3	0.5	1.72	0.03	7.90	0.25
TG-8A-07	229	0.282424	0.000019	0.002004	0.047809	-7.6	0.7	1.75	0.04	7.98	0.29

TG-8A-08	225	0.282352	0.000012	0.001182	0.027636	-10.1	0.4	1.90	0.03	7.32	0.40
TG-8A-09	217	0.282332	0.000017	0.001968	0.047416	-11.1	0.6	1.95	0.04	6.89	0.47
TG-8A-10	216	0.282343	0.000013	0.000998	0.023146	-10.6	0.5	1.92	0.03	7.26	0.49
TG-8A-12	226	0.282343	0.000014	0.001220	0.027937	-10.4	0.5	1.92	0.03	7.53	0.31
TG-8A-13	224	0.282463	0.000017	0.001083	0.024160	-6.2	0.6	1.65	0.04	7.02	0.28
TG-8A-15	224	0.282395	0.000018	0.000794	0.018198	-8.5	0.6	1.80	0.04	7.26	0.27
TG-8A-17	228	0.282455	0.000014	0.001254	0.030848	-6.4	0.5	1.67	0.03	7.62	0.16
TG-8A-18	224	0.282363	0.000016	0.001142	0.025999	-9.7	0.6	1.88	0.04	7.73	0.39
TG-8A-19	230	0.282405	0.000016	0.001079	0.024899	-8.1	0.6	1.78	0.04	7.63	0.33
TG-8A-20	231	0.282404	0.000016	0.001328	0.030760	-8.1	0.5	1.78	0.03	7.73	0.18

TL-13A₁, monzonitic granite, Wat Kio Kan; N 20°19'32", E 100°18'33"

TL-13A ₁ -01	213	0.282750	0.000013	0.002019	0.087803	3.6	0.5	1.02	0.03	6.48	0.27
TL-13A ₁ -02	219	0.282697	0.000013	0.001982	0.084151	1.9	0.5	1.14	0.03	6.97	0.29
TL-13A ₁ -04	233	0.282715	0.000015	0.002471	0.109000	2.7	0.5	1.10	0.03	6.90	0.25
TL-13A ₁ -05	223	0.282693	0.000014	0.001041	0.043274	1.9	0.5	1.14	0.03	7.17	0.22
TL-13A ₁ -06	219	0.282758	0.000016	0.001596	0.068991	4.1	0.6	1.00	0.04	6.63	0.24
TL-13A ₁ -07	215	0.282735	0.000015	0.001431	0.060114	3.2	0.5	1.05	0.03	6.98	0.29
TL-13A ₁ -08	218	0.282727	0.000018	0.001689	0.072082	3.0	0.6	1.07	0.04	6.32	0.40
TL-13A ₁ -09	218	0.282676	0.000016	0.001397	0.054784	1.2	0.6	1.18	0.03	5.89	0.47
TL-13A ₁ -12	217	0.282749	0.000008	0.002106	0.088601	3.7	0.3	1.02	0.02	5.88	0.35
TL-13A ₁ -13	246	0.282755	0.000020	0.001140	0.047234	4.6	0.7	0.98	0.04	6.53	0.23
TL-13A ₁ -14	246	0.282753	0.000012	0.001870	0.079535	4.4	0.4	1.00	0.03	6.02	0.28
TL-13A ₁ -15	240	0.282713	0.000007	0.002309	0.100179	2.8	0.2	1.10	0.02	6.05	0.36
TL-13A ₁ -16	237	0.282684	0.000007	0.001519	0.064183	1.9	0.2	1.15	0.02	6.26	0.27
TL-13A ₁ -18	228	0.282750	0.000018	0.001261	0.050267	4.0	0.6	1.01	0.04	6.62	0.16
TL-13A ₁ -19	231	0.282771	0.000016	0.001378	0.056928	4.8	0.6	0.96	0.04	6.73	0.39
TL-13A ₁ -20	229	0.282751	0.000017	0.001421	0.058757	4.1	0.6	1.01	0.04	6.63	0.33
TL-13A ₁ -21	233	0.282654	0.000016	0.001817	0.075691	0.7	0.6	1.23	0.04	6.73	0.18
TL-13A ₁ -22	232	0.282738	0.000015	0.002020	0.089230	3.6	0.5	1.04	0.03	7.16	0.17
TL-13A ₁ -23	228	0.282718	0.000017	0.001420	0.064134	2.9	0.6	1.08	0.04		

TG-27A, monzonitic granite, 20 km northeast toward Tak; N 17°07'54", E 99°06'11"

TG-27A-01	221	0.282634	0.000015	0.001168	0.028094	-0.2	0.5	1.27	0.03	6.38	0.24
TG-27A-02	223	0.282640	0.000009	0.001444	0.034113	0.0	0.3	1.26	0.02	5.61	0.32
TG-27A-03	219	0.282634	0.000008	0.000867	0.020924	-0.2	0.3	1.27	0.02	6.18	0.32

TG-27A-05	229	0.282638	0.000009	0.000802	0.018506	0.2	0.3	1.25	0.02	5.95	0.33
TG-27A-06	227	0.282611	0.000012	0.001477	0.035330	-0.9	0.4	1.32	0.03	6.10	0.32
TG-27A-08	216	0.282623	0.000009	0.002402	0.056921	-0.9	0.3	1.31	0.02	5.80	0.34
TG-27A-09	231	0.282583	0.000008	0.001003	0.024890	-1.8	0.3	1.38	0.02	5.73	0.23
TG-27A-10	234	0.282601	0.000012	0.002443	0.059336	-1.3	0.4	1.35	0.03	6.12	0.28
TG-27A-12	221	0.282601	0.000009	0.000932	0.022087	-1.3	0.3	1.34	0.02	6.12	0.27
TG-27A-14	224	0.282734	0.000014	0.000857	0.020156	3.4	0.5	1.04	0.03	5.55	0.30
TG-27A-15	227	0.282641	0.000008	0.000614	0.014349	0.2	0.3	1.25	0.02	5.67	0.29
TG-27A-16	219	0.282646	0.000020	0.000989	0.021765	0.2	0.7	1.24	0.04	5.72	0.43
TG-27A-17	230	0.282541	0.000012	0.000685	0.013791	-3.2	0.4	1.47	0.03	6.09	0.34
TG-27A-18	221	0.282632	0.000007	0.001241	0.031227	-0.3	0.2	1.28	0.02	5.72	0.16
TG-27A-19	222	0.282684	0.000007	0.001187	0.029705	1.6	0.2	1.16	0.02	5.57	0.25
TG-27A-20	226	0.282612	0.000012	0.001587	0.038230	-0.9	0.4	1.32	0.03	6.14	0.35
TG-27A-21	222	0.282630	0.000011	0.000470	0.011164	-0.2	0.4	1.27	0.02	5.48	0.28
TG-27A-22	230	0.282580	0.000007	0.001014	0.023571	-1.9	0.2	1.39	0.02	5.64	0.27
TG-27A-23	226	0.282610	0.000009	0.000906	0.021647	-0.9	0.3	1.32	0.02	5.59	0.17
TG-27A-24	219	0.282610	0.000010	0.001871	0.042087	-1.2	0.4	1.33	0.02	5.83	0.39

Table 3: Major oxides, trace elemental and Sr-Nd isotopic analytical results for the late Triassic granites from the Inthanon and Sukhothai zones in NW Thailand

Sample	TG-5A	TG-5G	TG-5B	TG-6A	TG-6B	TG-6E	TG-6G	TL-26A	TG-11A	TG-11C	TG-11D	TG-16A ₁	TG-16A ₂	TG-16B ₁	
	Fang Hotspring National Park				Southeast of Fang Hotspring National Park				Sleeping	Mae-Wiang Pa Pao 118 Highway			Khun Tan pluton		
	N19°57'57.75", E99°09'12.34"				N19°57'11.54", E99°09'38.84"				Buddha	N19°41'36.12", E99°25'05.35"			N18°27'21.63", E99°11'34.69"		
Group 1 samples: Triassic granites in the Inthanon zone to west of the Chiang Rai Fault in NW Thailand															
SiO ₂	69.11	76.38	69.78	72.25	67.41	68.31	69.98	69.91	70.09	69.09	65.66	70.95	70.78	68.95	
TiO ₂	0.30	0.09	0.67	0.33	0.69	0.62	0.60	0.40	0.50	0.52	0.62	0.63	0.61	0.65	
Al ₂ O ₃	14.69	12.47	13.58	13.97	14.67	14.80	13.99	14.78	13.57	14.38	15.55	12.54	13.56	14.00	
FeOt	1.94	0.37	4.24	1.71	4.28	3.66	3.76	2.90	2.84	2.93	3.36	3.93	3.26	3.49	
MgO	0.93	0.11	2.53	1.15	2.92	2.52	2.17	2.60	1.61	1.63	1.76	2.71	2.38	2.03	
CaO	0.46	0.14	0.35	0.89	1.96	1.17	1.27	1.63	1.63	2.31	1.24	2.41	2.79	1.33	
K ₂ O	10.10	8.85	3.93	6.97	4.44	4.96	3.63	2.35	5.71	4.29	5.13	3.25	3.19	4.81	
Na ₂ O	1.08	1.06	2.55	1.67	2.38	2.02	3.05	2.37	2.41	3.09	5.21	1.70	2.19	2.54	
P ₂ O ₅	0.31	0.08	0.17	0.16	0.14	0.17	0.16	0.10	0.15	0.14	0.13	0.35	0.35	0.26	
MnO	0.02	0.01	0.03	0.03	0.06	0.05	0.04	0.05	0.04	0.05	0.04	0.08	0.07	0.07	
LOI	1.07	0.53	2.12	0.90	1.01	1.69	1.35	2.48	1.44	1.63	1.47	1.13	0.68	1.83	
Total	99.99	100.09	99.95	100.03	99.95	99.97	100.01	99.57	100.01	100.05	100.17	99.67	99.85	99.96	
A/CNK	1.08	1.07	1.49	1.17	1.19	1.37	1.24	1.57	1.03	1.03	0.95	1.17	1.12	1.18	
A/NK	1.15	1.10	1.61	1.35	1.68	1.70	1.56	2.29	1.34	1.48	1.10	1.98	1.92	1.49	
Sc	13.8	10.3	15.4	10.2	13.5	12.3	12.8	2.5	12.6	13.0	20.8	13.4	13.3	13.2	
V	25.6	6.2	70.3	25.3	78.2	63.9	53.3	59.4	41.3	43.8	46.0	92.1	75.1	62.9	
Cr	52.7	12.0	83.4	37.4	113.4	101.3	76.1	31.1	39.2	41.4	47.3	71.7	63.1	53.2	
Co	2.58	0.23	5.65	2.99	11.58	9.17	8.76	4.43	8.98	6.77	7.94	12.04	10.85	5.42	
Ni	104.0	24.1	29.7	10.2	57.8	41.4	28.2	5.90	17.1	15.8	17.2	27.2	21.9	11.1	

Ga	11.31	6.00	18.38	16.19	18.87	17.51	15.22	8.98	15.57	16.98	16.56	17.71	19.02	17.92
Rb	449	349	262	199	209	263	174	42	288	286	224	283	279	232
Sr	110	65	87	91	125	123	208	153	110	92	136	136	142	243
Y	19.82	12.35	25.72	29.37	30.42	33.14	29.81	19.26	35.33	32.40	30.75	32.12	33.24	28.12
Zr	42.0	11.0	125	84	130	164	189	165	198	196	223	358	432	346
Nb	8.88	3.21	14.37	14.51	14.16	15.17	13.35	6.68	14.04	14.33	14.72	27.43	24.41	20.95
Cs	42.64	14.55	19.74	8.69	13.43	20.89	8.69	2.99	5.78	6.24	70.60	18.59	30.98	5.89
Ba	1412	709	768	700	1095	1148	802	281	994	409	846	378	368	973
La	10.54	8.41	35.38	28.37	46.58	47.41	42.54	25.90	40.41	43.94	43.78	37.90	49.94	43.90
Ce	22.91	17.06	71.38	57.16	88.89	93.29	84.58	52.20	83.79	87.89	90.02	86.10	107.46	84.87
Pr	2.86	1.87	8.27	6.73	10.37	11.00	9.61	6.47	10.12	10.40	10.49	10.35	12.96	10.72
Nd	10.84	6.58	30.16	24.35	37.16	39.32	35.03	23.10	34.95	38.51	38.08	40.97	50.54	41.87
Sm	2.66	1.37	6.18	5.50	7.51	7.49	7.23	4.33	7.49	8.04	7.85	9.32	10.39	8.48
Eu	0.96	0.49	1.07	0.83	1.38	1.32	1.00	0.81	1.11	0.95	1.07	0.91	0.98	1.34
Gd	2.62	1.49	5.65	4.88	6.63	6.89	6.16	3.91	6.54	6.50	7.07	7.70	8.24	6.71
Tb	0.62	0.33	0.87	0.91	1.06	1.12	0.99	0.64	1.14	1.12	1.12	1.27	1.30	1.05
Dy	3.81	2.25	4.57	5.31	5.67	6.34	5.29	3.52	6.35	5.86	6.26	6.47	6.70	5.51
Ho	0.84	0.51	1.01	1.13	1.22	1.39	1.20	0.71	1.41	1.32	1.25	1.30	1.35	1.13
Er	2.01	1.37	2.62	2.90	3.09	3.45	3.09	1.99	3.70	3.36	3.34	3.42	3.47	2.86
Tm	0.29	0.20	0.34	0.43	0.45	0.50	0.44	0.30	0.54	0.47	0.46	0.46	0.46	0.38
Yb	1.61	1.30	2.14	2.71	2.94	3.32	2.71	1.96	3.47	3.16	2.77	2.72	2.97	2.44
Lu	0.23	0.18	0.28	0.39	0.44	0.48	0.40	0.29	0.50	0.47	0.39	0.38	0.40	0.34
Hf	1.32	0.43	3.45	2.78	3.94	4.91	5.07	4.19	6.00	5.82	6.61	10.45	13.13	10.31
Ta	1.19	0.71	1.32	3.26	1.49	1.61	1.68	0.53	1.93	2.05	2.23	2.28	2.13	2.10
Pb	58.74	38.00	31.45	52.61	40.32	48.35	40.40	2.28	60.17	44.21	47.21	36.59	41.83	143.51
Th	3.91	6.27	22.76	17.98	26.65	30.57	28.55	8.71	32.99	33.88	35.75	63.65	90.02	53.21

U	3.76	5.63	4.29	7.38	8.43	6.82	6.49	2.07	9.15	9.09	11.63	14.23	18.97	9.15
$^{87}\text{Rb}/^{86}\text{Sr}$	11.855		8.701	6.376		6.213		7.558			6.010		2.771	
$^{87}\text{Sr}/^{86}\text{Sr}$	0.750914		0.746171	0.746945		0.747012		0.752917			0.745511		0.729765	
2σ	6		6	6		7		6			6		8	
$(^{87}\text{Sr}/^{86}\text{Sr})_i$	0.71382		0.718948	0.726993		0.727573		0.729269			0.726706		0.721094	
$^{147}\text{Sm}/^{144}\text{Nd}$	0.149		0.124	0.137		0.115		0.130			0.138		0.123	
$^{143}\text{Nd}/^{144}\text{Nd}$	0.511911		0.511808	0.511882		0.511842		0.511909			0.511921		0.511927	
2σ	4		4	4		4		4			4		3	
$\varepsilon\text{Nd (t)}$	-12.8		-14.1	-13.1		-13.3		-12.3			-12.3		-11.8	
T _{DM} (Ga)	2.92		2.28	2.51		2.03		2.26			2.47		2.05	

(to be continued)

	TG-16B ₃	TG-16B ₄	TG-30A	TG-30B ₁	TG-30B ₃	TG-30B ₄	TG-30B ₅	TG30B ₆	TG-30B ₇	TG-32A	TG-32D	TG-32B	TG-32C	TG-32D
Sample	Khun Tan pluton		N18°13'28"	Inthanon National Park							West of Nam Mae Chan			
			.50",E98°2'											
	N18°27'21.63", E99°11'34.69"		9'10.09"	N18°29'41.03", E98°40'03.95"							N18°13'28.50", E98°29'10.09"			
Group 1 samples: Triassic granites in the Inthanon zone to west of the Chiang Rai Fault in NW Thailand														
SiO ₂	71.69	72.55	72.42	73.76	74.21	73.47	73.82	73.55	73.55	72.42	73.84	76.05	72.71	73.84
TiO ₂	0.50	0.30	0.04	0.02	0.02	0.01	0.03	0.03	0.03	0.04	0.17	0.04	0.14	0.17
Al ₂ O ₃	13.50	14.61	15.36	15.22	15.41	14.93	15.33	15.20	15.11	15.36	14.14	14.17	15.17	14.14
FeOt	2.51	1.55	0.01	0.08	0.05	0.03	0.04	0.20	0.20	0.01	0.91	0.08	0.79	0.91
MgO	1.52	0.68	0.16	0.11	0.14	0.10	0.10	0.11	0.12	0.16	0.49	0.13	0.44	0.49
CaO	0.95	0.78	0.54	0.73	0.69	0.43	0.89	0.91	0.92	0.54	1.26	0.76	1.05	1.26
K ₂ O	5.06	5.66	9.15	7.04	6.54	8.71	6.50	6.41	6.50	9.15	6.17	5.33	6.91	6.17
Na ₂ O	2.68	2.92	2.30	2.78	2.69	2.14	3.16	3.12	3.07	2.30	2.72	3.44	2.62	2.72
P ₂ O ₅	0.19	0.15	0.07	0.03	0.03	0.03	0.03	0.03	0.03	0.07	0.11	0.02	0.05	0.11
MnO	0.04	0.03	0.01	0.04	0.05	0.06	0.02	0.02	0.03	0.01	0.01	0.01	0.01	0.01
LOI	1.42	0.89	0.25	0.37	0.47	0.27	0.32	0.41	0.41	0.25	0.35	0.23	0.30	0.35
Total	100.05	100.14	100.29	100.18	100.30	100.19	100.26	99.98	99.97	100.28	100.18	100.29	100.18	100.18
A/CNK	1.16	1.18	1.05	1.05	1.21	1.08	1.11	1.11	1.10	1.05	1.05	1.10	1.11	1.05
A/NK	1.36	1.33	1.12	1.12	1.34	1.15	1.25	1.26	1.25	1.12	1.27	1.24	1.28	1.27
Sc	12.5	11.4	11.8	12.4	9.70		10.2			11.8	9.90	9.30	11.4	9.90
V	46.8	16.2	2.70	7.30	1.00		1.00			2.70	10.7	0.10	9.90	10.7
Cr	38.3	10.4	5.90	13.1	4.80		6.10			5.9	12.3	4.10	14.6	12.3
Co	5.61	2.03	0.50	0.92	0.19		0.30			0.50	2.25	0.23	1.84	2.25
Ni	13.2	4.60	1.30	2.90	0.90		2.40			1.30	4.10	1.60	6.40	4.10

Ga	15.85	18.24	8.83	15.41	15.54	13.37	8.83	12.68	12.47	13.6	12.68
Rb	282	329	274	280	330	303	274	204	259	226	204
Sr	138	105	151	122	86	96	151	140	60	140	140
Y	21.52	19.48	2.96	28.14	18.3	18.78	2.96	10.04	14.24	18.48	10.04
Zr	221	138	7.0	59.0	27.0	29	7.0	56	13	57	56
Nb	15.89	15.35	1.20	6.45	9.56	5.48	1.20	6.04	11.08	6.28	6.04
Cs	11.42	13.48	2.12	5.34	6.51	5.63	2.12	3.21	7.07	2.49	3.21
Ba	871	506	884	491	335	372	884	612	124	700	612
La	44.95	33.72	2.66	7.93	6.93	6.14	2.66	16.18	5.90	14.33	16.18
Ce	94.28	70.78	4.49	15.08	14.74	11.99	4.49	32.10	11.81	28.25	32.10
Pr	11.17	8.17	0.50	1.89	1.78	1.40	0.50	3.71	1.37	3.16	3.71
Nd	42.52	30.12	1.76	6.90	6.27	4.90	1.76	13.18	5.10	11.23	13.18
Sm	7.85	6.11	0.39	2.15	2.29	1.69	0.39	2.88	1.66	2.41	2.88
Eu	1.23	0.73	0.08	0.46	0.25	0.27	0.08	0.72	0.19	0.81	0.72
Gd	6.14	4.75	0.42	2.38	2.00	1.77	0.42	2.53	1.52	2.44	2.53
Tb	0.92	0.74	0.09	0.64	0.48	0.45	0.09	0.42	0.37	0.46	0.42
Dy	4.35	3.81	0.53	4.26	2.92	2.88	0.53	2.15	2.35	2.90	2.15
Ho	0.87	0.74	0.11	0.93	0.61	0.65	0.11	0.37	0.50	0.64	0.37
Er	2.23	2.04	0.28	2.58	1.68	1.75	0.28	0.84	1.29	1.69	0.84
Tm	0.31	0.29	0.04	0.42	0.27	0.30	0.04	0.10	0.22	0.27	0.10
Yb	1.99	1.93	0.23	3.03	1.91	1.89	0.23	0.56	1.44	1.62	0.56
Lu	0.28	0.26	0.03	0.48	0.29	0.27	0.03	0.07	0.20	0.23	0.07
Hf	6.47	4.21	0.25	2.72	1.97	1.65	0.25	1.83	1.06	1.92	1.83
Ta	1.72	1.96	0.12	0.67	0.82	0.62	0.12	0.34	1.86	0.41	0.34
Pb	63.53	68.13	98.52	57.09	47.56	49.10	98.52	75.21	83.88	83.69	75.21
Th	47.80	40.04	1.42	8.83	6.95	6.01	1.42	12.16	8.37	11.82	12.16

U	9.12	9.68	0.56	8.51	8.73	8.41	0.56	2.56	2.53	3.23	2.56
$^{87}\text{Rb}/^{86}\text{Sr}$			5.284		11.157		5.284			6.010	
$^{87}\text{Sr}/^{86}\text{Sr}$			0.727641		0.759769		0.727641			0.745511	
2σ			8		6		8			6	
$(^{87}\text{Sr}/^{86}\text{Sr})_i$			0.711108		0.724858		0.711108			0.726706	
$^{147}\text{Sm}/^{144}\text{Nd}$			0.135		0.124		0.135			0.138	
$^{143}\text{Nd}/^{144}\text{Nd}$			0.511980		0.511988		0.511942			0.511921	
2σ			4		4		5			4	
$\varepsilon\text{Nd (t)}$			-11.1		-12.0		-11.9			-12.3	
T _{DM} (Ga)			2.28		2.11		2.36			2.47	

(to be continued)

	TG-42A	TG-42B	TG-42D	TG-52A	TG-53A	TG-8A	TG-8C	TG-8D	TG-8F	TL13A ₁	TL13A ₂	TL15A ₁	TL15A ₂	TG-26C						
	85km Marker along 1095 Highway				Mae Chan pluton				Wat Kio Kan		Goldern Triangle Park		LangSang							
Sample	Doi Inthanon				N20°07'34.9", E99°51'59.35"				N20°19'31.9", E100°18'33.4"		N20°21'35.3", E100°04'44.4"		N16°46'58.94", E99°01'3.91"							
	N19°17'03.68", E98°29'08.8"							Group 1: Triassic granites in the Inthanon zone												
Group 2 samples: Triassic granites in the Sukhothasi zone to east of the Chiang Rai Fault in NW Thailand																				
SiO ₂	71.27	69.01	69.41	71.96	71.46	68.64	65.91	65.81	65.48	75.82	75.62	70.51	70.23	70.46						
TiO ₂	0.43	0.56	0.55	0.25	0.38	0.68	0.65	0.61	0.62	0.13	0.12	0.48	0.49	0.60						
Al ₂ O ₃	14.04	14.81	14.54	14.80	14.13	14.37	15.45	15.77	15.40	12.75	12.89	13.98	14.10	13.94						
FeOt	2.49	3.33	3.33	1.50	2.39	3.56	3.49	3.36	3.38	1.16	1.10	3.96	3.95	3.38						
MgO	1.70	2.00	2.06	0.70	1.39	1.69	1.94	1.80	1.87	0.12	0.10	1.55	1.62	1.91						
CaO	1.57	1.81	1.45	1.56	1.84	3.36	2.95	2.77	4.03	0.90	0.85	3.02	3.09	2.47						
K ₂ O	4.40	4.64	4.32	4.16	4.12	3.16	4.63	4.93	3.85	5.36	5.63	3.60	3.65	3.84						
Na ₂ O	2.72	2.88	2.68	3.84	2.89	3.76	3.00	3.19	3.29	3.17	3.18	2.14	2.09	2.75						
P ₂ O ₅	0.21	0.17	0.20	0.09	0.11	0.15	0.21	0.21	0.22	0.01	0.01	0.07	0.07	0.19						
MnO	0.04	0.05	0.05	0.04	0.04	0.06	0.06	0.05	0.05	0.02	0.02	0.06	0.06	0.05						
LOI	1.20	0.76	1.42	0.61	0.77	0.65	1.73	1.52	1.85	0.76	0.69	0.58	0.60	0.45						
Total	100.07	100.03	100.01	99.51	99.51	100.08	100.01	100.03	100.04	100.18	100.18	99.96	99.96	100.04						
A/CNK	1.16	1.13	1.24	1.08	1.12	0.91	1.01	1.01	0.91	1.01	1.00	1.08	1.08	1.06						
A/NK	1.52	1.52	1.60	1.37	1.53	1.50	1.55	1.49	1.60	1.16	1.14	1.88	1.91	1.60						
Sc	11.6	12.2	11.5	3.9	6.5	13.5	13.1	13.9	13.1	4.4	10.8	11.9	12.2	11.3						
V	34.3	48.8	48.2	26.9	44.2	55.3	64.6	67.3	63.9	0.70	0.90	59.8	59.0	46.3						
Cr	44.8	63.4	60.6	22.2	54.0	25.3	30.2	29.4	31.7	2.00	1.70	22.4	23.3	51.7						
Co	7.67	8.08	5.71	2.92	7.41	8.41	9.3	8.6	9.48	0.39	0.54	7.68	7.80	8.15						
Ni	23.1	26.5	20.7	4.20	15.7	13.5	16.6	15.4	16.9	0.60	0.30	9.00	9.60	20.9						

Ga	17.06	18.48	19.35	20.65	17.02	17	16.04	16.33	17.7	7.16	12.95	13.21	13.01	16.73
Rb	231	253	248	136	199	178	196	198	197	155	276	146	148	211
Sr	124	142	128	406	138	155	374	365	401	25	37	135	133	157
Y	30.01	28.51	29.24	8.39	22.29	24	26.11	24.08	23.32	12.42	32.68	13.13	12.04	19.93
Zr	365	179	214	111	124	258	270	288	288	83	163	124	110	92
Nb	12.87	15.03	16.47	6.38	10.39	15.93	15.67	14.33	14.28	12	13.22	7.09	7.11	18.91
Cs	10.62	11.49	9.87	6.78	11.01	11.13	3.02	3.05	3.54	3.70	8.00	10.41	10.69	7.83
Ba	707	904	644	771	740	395	1788	1842	1171	99	160	566	590	866
La	49.54	49.35	51.12	16.80	37.23	45.94	62.05	58.72	58.90	17.56	47.34	23.23	22.55	14.69
Ce	100.52	99.80	101.17	34.99	74.33	85.41	116.74	110.42	111.25	39.03	91.76	40.93	38.65	30.94
Pr	11.82	11.42	11.89	4.24	9.16	9.81	13.49	12.79	12.72	4.55	10.35	4.52	4.21	3.97
Nd	42.41	41.65	43.43	16.26	34.11	35.24	47.45	44.67	44.36	16.28	37.31	16.46	15.07	15.95
Sm	8.13	8.04	8.58	3.11	6.36	6.76	8.06	7.84	7.44	3.26	7.02	2.95	2.76	4.11
Eu	1.13	1.20	1.06	0.46	0.99	1.13	1.77	1.72	1.56	0.22	0.42	1.01	0.93	1.09
Gd	6.76	6.87	7.19	2.38	5.30	6.06	7.11	6.84	6.38	2.70	6.25	2.60	2.56	3.76
Tb	1.06	1.05	1.11	0.34	0.83	0.92	0.99	0.91	0.89	0.43	0.97	0.41	0.39	0.69
Dy	5.51	5.37	5.42	1.70	4.41	4.93	4.91	4.42	4.06	2.25	5.25	2.25	2.05	3.71
Ho	1.13	1.12	1.11	0.31	0.87	1.01	1.03	0.91	0.90	0.54	1.20	0.50	0.47	0.76
Er	2.90	2.89	2.93	0.78	2.24	2.54	2.77	2.43	2.43	1.48	3.26	1.41	1.42	1.88
Tm	0.43	0.39	0.40	0.11	0.32	0.32	0.36	0.35	0.33	0.22	0.50	0.23	0.22	0.24
Yb	2.79	2.50	2.55	0.67	1.95	2.04	2.37	2.27	2.16	1.52	3.07	1.60	1.49	1.41
Lu	0.42	0.35	0.36	0.10	0.30	0.31	0.34	0.34	0.31	0.21	0.47	0.25	0.24	0.19
Hf	10.11	5.07	5.91	3.43	3.51	7.45	7.61	7.89	8.07	3.12	5.98	3.77	3.35	2.56
Ta	1.55	1.70	1.89	0.64	1.22	1.52	1.89	1.78	1.71	1.32	1.34	0.53	0.55	1.22
Pb	43.55	44.30	64.51	33.80	35.49	45.55	50.07	58.29	53.34	15.60	36.49	26.16	26.51	31.11
Th	29.54	29.79	32.38	8.63	20.54	46.15	43.15	42.93	46.06	13.00	32.53	7.65	6.79	21.16

U	10.75	11.96	9.02	3.81	4.57	11.24	8.82	9.28	8.26	3.94	7.82	2.69	2.04	4.10
$^{87}\text{Rb}/^{86}\text{Sr}$		5.163		0.968	4.204	3.313		1.569		17.773		3.135		3.892
$^{87}\text{Sr}/^{86}\text{Sr}$		0.744117		0.721176	0.725630	0.730255		0.732694		0.767342		0.721679		0.725557
2σ		6		6	6	7		6		9		6		6
$(^{87}\text{Sr}/^{86}\text{Sr})_i$		0.727963		0.718147	0.712475	0.719889		0.727785		0.711733		0.71187		0.713379
$^{147}\text{Sm}/^{144}\text{Nd}$		0.117		0.116	0.113	0.116		0.106		0.121		0.108		0.156
$^{143}\text{Nd}/^{144}\text{Nd}$		0.511886		0.511971	0.511933	0.512028		0.511942		0.512048		0.511958		0.512060
2σ		4		5	4	4		5		3		3		4
$\varepsilon\text{Nd (t)}$		-12.4		-10.8	-11.4	-9.6		-11.0		-9.4		-10.8		-10.1
T _{DM} (Ga)		1.99		1.84	1.84	1.75		1.72		1.82		1.73		2.88

(to be continued)

	TG-27A	TG-27B	TG-27D	TG-29B ₁	TG-29B ₃	TG-29B ₄
Sample	Northwest to Tak			LamPang		
	N17°07'54.45", E99°06'10.84"			N17°28'19.91", E99°11'01.6"		
Group 2 samples: Triassic granites in the Sukhothasi zone						
SiO ₂	74.06	71.95	72.14	73.06	74.69	74.98
TiO ₂	0.26	0.28	0.29	0.25	0.26	0.22
Al ₂ O ₃	13.38	14.90	14.70	12.87	13.08	12.74
FeOt	1.17	1.39	1.48	2.34	2.29	1.97
MgO	0.51	0.55	0.60	0.43	0.38	0.41
CaO	1.38	1.45	1.50	2.48	2.22	2.10
K ₂ O	5.31	5.16	4.87	4.24	4.54	4.25
Na ₂ O	3.09	3.70	3.77	2.49	2.43	2.11
P ₂ O ₅	0.05	0.06	0.06	0.03	0.04	0.03
MnO	0.06	0.06	0.07	0.04	0.03	0.05
LOI	0.90	0.71	0.72	1.90	0.33	1.49
Total	100.17	100.20	100.20	100.14	100.29	100.34
A/CNK	1.00	1.04	1.03	0.97	1.01	1.07
A/NK	1.23	1.28	1.28	1.48	1.47	1.58
Sc	9.0	8.3	9.9	14.2	15.9	16.3
V	14.5	15.2	16.1	7.5	8.2	9.0
Cr	8.10	8.80	7.60	5.90	9.30	40.8
Co	1.31	1.3	1.53	1.36	1.44	1.74
Ni	3.53	2.54	1.81	0.92	2.54	23.1
Ga	13.56	14.77	15.79	11.09	11.49	12.01
Rb	313	293	306	44	53	52

	165	165	172	72	61	77
Sr	165	165	172	72	61	77
Y	20.05	18.02	17.64	29.52	26.43	30.67
Zr	127	151	145	111	124	139
Nb	16.08	17.13	18.87	3.41	3.97	3.8
Cs	8.60	8.84	12.7	3.35	3.76	4.39
Ba	645	591	571	164	183	177
La	38.31	37.61	48.03	16.42	18.14	12.17
Ce	59.53	61.45	74.81	32.34	34.55	23.84
Pr	6.07	6.18	7.05	4.02	4.16	2.96
Nd	18.56	19.00	21.45	15.82	16.18	11.70
Sm	3.08	3.16	3.48	3.87	3.58	2.95
Eu	0.58	0.60	0.66	0.80	0.74	0.71
Gd	3.02	2.76	3.26	3.79	3.64	3.26
Tb	0.48	0.44	0.45	0.80	0.71	0.73
Dy	2.72	2.50	2.57	4.98	4.31	4.73
Ho	0.63	0.56	0.58	1.16	1.00	1.11
Er	2.00	1.77	1.74	3.16	2.70	3.13
Tm	0.33	0.30	0.29	0.48	0.45	0.48
Yb	2.15	2.12	2.04	3.30	2.90	3.21
Lu	0.35	0.34	0.35	0.51	0.45	0.49
Hf	3.80	4.20	4.23	3.27	3.40	3.55
Ta	1.74	1.90	1.95	0.30	0.32	0.31
Pb	48.78	60.82	63.50	3.00	2.60	2.63
Th	41.49	53.44	49.46	7.02	5.84	5.35
U	19.71	12.51	15.81	1.52	1.38	1.42
⁸⁷ Rb/ ⁸⁶ Sr	5.506			1.773		

$^{87}\text{Sr}/^{86}\text{Sr}$	0.729530	0.712811
2σ	6	7
$(^{87}\text{Sr}/^{86}\text{Sr})_i$	0.712302	0.707264
$^{147}\text{Sm}/^{144}\text{Nd}$	0.100	0.148
$^{143}\text{Nd}/^{144}\text{Nd}$	0.512031	0.512141
2σ	4	4
$\epsilon_{\text{Nd}}(t)$	-9.1	-8.3
T_{DM} (Ga)	1.51	2.34

Highlights

- The granitic rocks in the Inthanon and Sukhothai zones yield the zircon U-Pb crystallization ages of 230-200 Ma.
- The Inthanon and Sukhothai granites show similar elemental but distinct Sr-Nd-Hf-O isotopic compositions, respectively.
- The Inthanon and Sukhothai granites mainly originated from the supracrustal and underplating rocks, respectively.
- The Inthanon zone represents the main suture zone of the eastern Paleotethyan Ocean in NW Thailand
- The syn- and post-collisional events in NW Thailand occurred at ~237-230 Ma and ~200-230 Ma, respectively,